In Vivo Dendritic Dynamics of Somatostatin-Expressing Interneurons (SST-INs) In the Primary Motor Cortex (M1) During Motor Learning

Minh Nhi Tran

Thesis submitted to the University of Ottawa in partial Fulfillment of the requirements for the Master of Science's degree in Neuroscience

Department of Cellular and Molecular Medicine-Neuroscience
Faculty of Medicine
University of Ottawa

Abstract:

The primary motor cortex (M1) is critical for motor learning. Within M1, excitatory pyramidal neurons (PyrNs) undergo network re-organizations, forming task-specific ensembles. This process was recently discovered to be modulated by a functionally distinct ensemble of somatostatin-expressing inhibitory neurons (SST-INs) in M1 that predominantly express neuronal PAS domain 4 (NPAS4) upon motor learning. NPAS4+ SST-INs reduced inhibition onto postsynaptic PyrNs, facilitating circuit reorganization, and thus, motor learning. NPAS4+SST-IN ensemble hints at learning-associated input integration in SST-INs, however, the underpinning of this process remains unclear. To investigate this, I employ *in vivo* two photon Ca^{2+} imaging in awake mice to chronically monitor dendritic and synaptic activity of SST-INs throughout training for head-restrained bi-directional disk task, followed by identification of NPAS4+ SST-IN ensemble in M1. Building upon finding of branch-specific Ca^{2+} spikes on layer 5 PyrNs' apical dendrites in M1during motor learning, which induces potentiation of learning-related spines, I hypothesize that motor learning-induced dendritic Ca^{2+} activity will trigger and maintain experience-dependent synaptic plasticity in dendrites of NPAS4+ SST-INs. We observed two distinct SST-IN populations during motor training: neurons showing increased ('positive') or decreased ('negative') dendritic activity. Task-specific NPAS4+ SST-INs displayed a nuanced pattern of synaptic integration. In the early training phase, these neurons exhibited broader, non-specific synaptic engagement, characterized by higher spine-dendrite co-activity. As training progressed, we observed a selective refinement of synaptic connections, suggesting an active mechanism of circuit optimization. Overall, this research elucidates dendritic and synaptic plasticity of SST-INs during motor learning, offering insights into neural plasticity and potential therapeutic strategies for neurological injury rehabilitation.

Introduction:

The role of Primary Motor Cortex (M1) in Motor Learning:

Motor learning is the ability for one to adapt actions and movements to different situations and environments. Past studies have attributed the primary motor cortex (M1) as one of the essential brain regions for this process, as disruption of M1 using pharmacological or optogenetic inactivation reduced motor functions in animals (Guo et al., 2015; Otchy et al., 2015; Peters et al., 2014). Intriguingly, damaging M1 prior to motor learning incapacitates task acquisition but does not impact animal's daily motor movements (Peters et al., 2014; Kawai et al., 2015).

Over the past decade, extensive research has been conducted to identify the physical substrate for memories and found that motor skill learning induces the formation and selective maintenance of experience-dependent dendritic spine reorganization among layer 2/3 and layer 5 pyramidal neurons (L2/3 and L5 PyrNs) in M1. *In vitro* study by Harms and colleagues (2008) found an increase in spine size, but not the density, in L1 of M1 in rats following motor learning, suggesting enhanced synaptic strength. In line with Harms' work, studies utilizing two photon structural imaging to chronically monitor spine activity in awake mice during motor training confirmed rapid formation of new spines during the initial phase of training, followed by selective spine elimination on dendritic branches of L5 PyrNs of M1 (Xu et al., 2009; Yang et al., 2009); hence, synaptic remodelling of excitatory connectivity in M1 gives rise to task-specific motor ensembles for future retrieval (Hayashi-Takagi et al., 2015).

In conjunction, inhibitory circuits play a critical regulatory role in motor learning-related plasticity. Studies have shown that certain forms of synaptic potentiation in motor cortex can only occur when inhibition is experimentally reduced (Hess & Donoghue, 1994). More recently,

Chen and colleagues (2015) demonstrated that during motor skill acquisition, the formation of new dendritic spines coincides with a reduction in inhibitory inputs from somatostatin-expressing interneurons specifically targeting apical dendrites. This balanced excitatory-inhibitory reorganization appears precisely regulated, as experimentally altering somatostatin neuron activity during learning disrupted both spine dynamics and skill acquisition. Interestingly, these same manipulations had no effect after learning was complete, suggesting a time-limited role for inhibitory plasticity in the learning process. The inhibitory changes may themselves be orchestrated through sequential modifications of connections onto inhibitory neurons during different learning phases (Donato et al., 2013).

Functional imaging studies have revealed that motor learning induces complex changes in neuronal activity patterns. While individual neurons show variable relationships to movement, population-level analyses demonstrate increasing predictive power for movement success with training (Laubach et al., 2000). Longitudinal Ca^{2+} imaging has shown that the motor cortex develops new and more consistent activity patterns associated with learned movements (Peters et al., 2014; Huber et al., 2012). These functional adaptations appear layer-specific, with deeper cortical layers showing net increases in movement-related information, while superficial layers maintain balanced increases and decreases (Masamizu et al., 2014), suggesting layer-specific functional role in motor learning.

Activity-dependent Dendritic and Synaptic Plasticity:

Dendritic activity represents a crucial function for neural computation, extending far beyond passive signal propagation. Although action potentials typically originate in the axon initial segment (Stuart et al., 1997a; Kole et al., 2007), dendrites actively shape neuronal output through various mechanisms. Dendrites generate three primary types of regenerative events:

sodium spikes, Ca^{2+} spikes, and NMDA spikes (Schiller et al., 2000; Golding & Spruston, 1998; Larkum et al., 1999b). These dendritic spikes transform branches into computational subunits capable of supralinear integration when inputs are spatially clustered (Polsky et al., 2004; Losonczy & Magee, 2006), fundamentally altering our understanding of neuronal computation.

In vivo research using advanced methodologies, including two-photon Ca^{2+} imaging, patch-clamp recordings, and genetically encoded indicators, has revealed the dynamic nature of dendritic activity during behavior. Dendrites integrate synaptic inputs with remarkable flexibility, operating in sublinear, linear, or supralinear regimes depending on context (Longordo et al., 2013; Lavzin et al., 2012; Palmer et al., 2014). Ca^{2+} imaging has captured branch-specific activity patterns during sensory processing, with different stimuli evoking distinct spatial patterns of dendritic Ca^{2+} transients (Jia et al., 2010). Direct dendritic recordings have demonstrated that dendritic spikes enhance stimulus selectivity during sensory processing, including whisker sensing, object localization, and somatosensory perception (Lavzin et al., 2012; Xu et al., 2012; Smith et al., 2013).

The role of dendritic activity in learning and memory formation has emerged as particularly significant. Two-photon imaging has revealed that motor training induces branch-specific dendritic Ca^{2+} spikes in layer 5 pyramidal neurons, which potentiate task-relevant dendritic spines (Cichon & Gan, 2015). When the spatial segregation of these Ca^{2+} spikes is disrupted, animals fail to learn multiple motor skills, demonstrating the causal importance of compartmentalized dendritic activity. In the hippocampus, basal dendritic Ca^{2+} transients strongly correlate with place field properties during navigation (Sheffield & Dombeck, 2015), while clustered synaptic plasticity during learning has been observed across multiple brain regions (Fu et al., 2012; Takahashi et al., 2012). Dendritic NMDA receptor activation appears

critical for these learning processes, as postsynaptic NMDA-dependent spiking is necessary for certain forms of plasticity *in vivo* (Gambino et al., 2014).

Inhibitory control of dendritic activity adds another layer of computational sophistication. Different interneuron subtypes selectively target specific dendritic compartments, with somatostatin-expressing interneurons (SST-INs) inhibiting distal dendrites and parvalbumin-expressing interneurons (PV-INs) targeting perisomatic regions (Gentet et al., 2012; Murayama et al., 2009). This inhibitory control regulates dendritic spike generation and propagation, thereby fine-tuning information processing at the dendritic level. Together, these findings highlight dendrites as active computational elements whose distinct activity patterns directly shape neural processing, stimulus selectivity, and learning in the intact brain.

Interaction of Dendritic Activity and Inhibitory Control During Motor Learning:

The acquisition and consolidation of motor skills through repetitive practice provides a compelling example of how dendritic activity and inhibitory control interact during learning. Motor learning triggers not only excitatory network reorganization but also subtype-specific inhibitory reorganization of local interneurons (Chen et al., 2015). During motor training, axonal bouton density of SST-INs rapidly decreases initially, whereas bouton density of PV-INs increases throughout learning (Chen et al., 2015), exerting differential inhibition on pyramidal neurons. This dynamic inhibitory remodeling complements the branch-specific dendritic Ca^{2+} spikes observed in layer 5 pyramidal neurons of the primary motor cortex (M1) during motor skill acquisition. These spatially segregated Ca^{2+} spikes potentiate task-related dendritic spines, creating a cellular substrate for motor memory encoding (Cichon & Gan, 2015). Similar input-specific dendritic Ca^{2+} activity patterns appear in the primary visual cortex (V1), where different drifting gratings evoke distinct local dendritic Ca^{2+} signals that map single synaptic inputs across

the dendritic tree (Jia et al., 2010). Collectively, these findings underscore the importance of precisely regulated dendritic Ca^{2+} dynamics in both learning processes and sensory information processing.

Inhibitory Synaptic Plasticity: Molecular Mechanisms and Functional Roles

Inhibitory synaptic plasticity (ISP) differs markedly from its excitatory counterpart, as evidenced by the four distinct spike-timing-dependent plasticity rules observed in GABAergic synapses. According to Hennequin et al. (2017), these rules vary considerably across brain regions, with some showing depression when inhibitory spikes occur near postsynaptic bursts, others displaying asymmetric strengthening/weakening depending on spike order, and yet others affecting either synaptic conductance or chloride reversal potentials. Unlike the relatively consistent Hebbian rules observed in excitatory synapses, inhibitory plasticity appears to be context-dependent, influenced by factors beyond simple spike timing.

Functionally, ISP plays crucial roles beyond simple synaptic modification. It enables network stabilization by preventing runaway excitation while enabling proper signal processing, creates signal gating through precise excitation-inhibition balance, and participates directly in memory formation. Rather than memories being stored exclusively in excitatory connections, Hennequin et al. (2017) propose that memory engrams comprise both excitatory and inhibitory neurons, with ISP creating assembly-specific feedback loops that maintain activity-silent memories that can be reactivated when balance is disrupted. Castillo et al. (2011) further delineate the diverse mechanisms underlying ISP, identifying several distinct forms operating at both presynaptic and postsynaptic loci. Presynaptically, endocannabinoid-mediated inhibitory-LTD (Chevaleyre & Castillo, 2003), BDNF-TrkB-mediated I-LTP (Inagaki et al., 2008), nitric oxide-triggered I-LTP (Nugent et al., 2007), and NMDAR-dependent plasticity (Lien et al.,

2006) act through retrograde or direct signaling pathways, while postsynaptically, changes in GABAAR trafficking (Ouardouz & Sastry, 2000), receptor phosphorylation (Kano et al., 1996), and chloride transporter activity (Woodin et al., 2003) enable a rich repertoire of inhibitory control that is central to complex neural circuit functions, including memory.

Activity-dependent Expression of Neuronal PAS domain 4 (NPAS4) in Task-related Plasticity:

Interestingly, SST-INs predominantly regulate spine reorganization, synaptic potentiation, and sequential activity patterns of downstream PyrNs during motor learning (Cichon and Gan, 2015; Chen et al., 2015; Adler et al., 2019). These neural dynamics provide a foundation for understanding the broader mechanisms of neural plasticity and memory formation.

The conversion of transient experiences into enduring memory involves a complex process of neural network modification, fundamentally dependent on activity-dependent gene transcription. Initial neuronal responses to sensory and behavioral inputs trigger a sophisticated molecular cascade that transforms momentary experiences into long-term memories, building upon the synaptic reorganization initiated by neural interneurons.

The process is characterized by two critical stages of gene expression. First, immediate early genes (IEGs) are rapidly activated within minutes, driven by intracellular calcium signaling and occurring without new protein synthesis. These IEGs then initiate a secondary gene expression wave that requires protein synthesis and facilitates critical cellular functions such as synaptic modification and memory consolidation, further elaborating on the molecular mechanisms underlying neural adaptation.

Notably, key IEGs like Fos, Arc, and Zif268 have been extensively studied for over two decades, representing a pivotal molecular link between neural experience and adaptive

neuroplasticity. Their near-instantaneous activation provides neuroscientists with a robust method to identify neuronal ensembles responsible for memory encoding, complementing the understanding of neural circuit dynamics.

Lin et al. (2008) and Bloodgood et al. (2013) established NPAS4 as a critical activity-dependent transcription factor regulating inhibitory synapse development during learning. NPAS4 is uniquely induced by Ca^{2+} influx following excitatory synaptic activity, unlike other transcription factors that respond to various stimuli. Its expression is transient and occurs predominantly in excitatory neurons, particularly in hippocampal CA1 pyramidal neurons following enriched environment exposure or seizure activity, extending the molecular insights into neural plasticity.

Using RNAi in cultured hippocampal neurons, Lin et al. demonstrated that NPAS4 critically regulates inhibitory synapse formation. NPAS4 knockdown significantly reduced inhibitory synapses, primarily affecting postsynaptic specializations. Electrophysiological recordings confirmed decreased functional inhibitory connections, while NPAS4 overexpression increased them, providing direct evidence of NPAS4's role in synaptic modulation.

Building on these findings, Bloodgood et al. revealed that NPAS4 performs domain-specific regulation of inhibition. Through AAV-Cre-GFP delivery to Npas4 conditional mice and layer-specific stimulation, they discovered that NPAS4 coordinates inhibitory circuit redistribution—increasing somatic inhibition while decreasing apical dendritic inhibition. GFP-gephyrin quantification confirmed this pattern, showing NPAS4-knockout neurons had fewer somatic but more dendritic inhibitory synapses, further elucidating the complex mechanisms of neural circuit reorganization.

Both studies identified BDNF as a key NPAS4 target, with Bloodgood et al. demonstrating that BDNF specifically mediates somatic inhibition. This domain-specific regulation serves a crucial function in learning: restricting neuronal output while creating a dendritic environment conducive to plasticity. This mechanism allows selective integration of inputs during learning while maintaining network stability. NPAS4 thus acts as a molecular switch orchestrating inhibitory circuit reorganization to optimize conditions for synaptic plasticity. Building upon these foundational insights, recent investigations have further elucidated NPAS4's specific role in motor learning.

A recent study from our lab identified neuronal PAS domain 4 (NPAS4), an activity-dependent transcription factor selectively expressed in a sub-population of SST-INs during a pellet reaching task (Yang et al., 2022). To investigate how NPAS4 mediates motor learning, Yang et al. (2022) performed SST-specific deletion of NPAS4, which impaired spine remodeling of downstream PyrNs and disrupted the animal's ability to learn reach-and-grasp movements. Using *in vivo* two-photon imaging to track SST-IN activity across training sessions, we discovered that learning-induced NPAS4 expression forms functionally distinct SST-IN ensembles with significantly reduced activity during reach-and-grasp movements. This task-elicited NPAS4 expression activates downstream transcriptional pathways that alleviate inhibition from SST-INs onto postsynaptic PyrNs, allowing proper induction and stabilization of learning-relevant dendritic spines (Yang et al., 2022).

Research Statement:

Learning-induced subtype-specific plasticity of INs and formation of functionally distinct NPAS4+ SST-IN ensembles in M1 suggest integration of task-related inputs at the dendritic domain of SST-INs. However, whether and how task-related inputs are consolidated on the

dendritic domain of SST-INs during motor learning remains unclear. This question drives my MSc project, in which I will employ *in vivo* two-photon Ca^{2+} imaging in awake mice to chronically monitor the activity of dendrites and spines of SST-INs during the bi-directional spinning disk motor task.

Aim and Hypothesis:

Aim:

1. Characterize in vivo dendritic and synaptic Ca^{2+} activity during motor learning
2. Examine task-related dendritic and synaptic modulation of NPAS4+ SST-INs in M1 during motor skill acquisition

Hypothesis:

I hypothesize that learning-induced dendritic Ca^{2+} dynamics selectively facilitate synaptic potentiation within NPAS4+ SST-INs, thereby mediating experience-dependent synaptic refinement and enabling task-specific circuit reorganization in M1.

Results:

Behavioral Task and Learning Metrics

Mice were trained on the novel, non-reward-associated head-fixed motor learning paradigm, which involved running on a bidirectional rotating disk (Figure 1A). The training protocol consisted of daily one-hour sessions over a 12-day period. Running epochs (REs) were defined as instances where mice surpassed a predetermined velocity threshold for 3 or more seconds (see Methods). Performance in the bidirectional running disk task was assessed using multiple behavior-based learning metrics, namely the 4-fold increase in total distance traveled across training sessions (Figure 1B). This specific parameter was selected as a performance indicator because its trajectory across sessions effectively delineates the development of running capability and execution proficiency.

The 12-day training period was divided into distinct learning phases: the 'naïve stage' (days 1–3), during which mice struggled to position themselves effectively to run on the disk, and the 'expert stage' (days 10–12), when mice had mastered the task. Notably, this head-fixed paradigm requires animals to learn an alternative running posture, necessitating voluntary and intentional movements that specifically engage the motor cortex, making it an ideal model for studying learning-induced plasticity in motor circuits.

Characterization of Dendritic and Synaptic Ca^{2+} Events

For chronic monitoring of somatostatin-expressing interneurons (SST-INs), we performed craniotomy surgery wherein a mixture of adeno-associated virus (AAV) encoding Flp-dependent Cre recombinase and Cre-dependent genetically encoded Ca^{2+} indicator (GECI) GCaMP6s was injected into the primary motor cortex (M1) region of SST-Flp mice (or alternatively, Cre-dependent Flp recombinase and Flp-dependent GCaMP6s for SST-Cre mice).

Two-photon Ca^{2+} imaging facilitated the observation of SST-IN activity dynamics in awake mice during training for a bidirectional running disk task.

Acquired imaging data underwent motion correction, followed by manual selection of regions of interest (ROIs) corresponding to dendritic shafts and spines using custom MATLAB programs. For each recorded dendritic segment, we delineated a region covering approximately 30 μm of the parent dendritic shaft, carefully excluding all visible spines to ensure accurate estimation of global dendritic Ca^{2+} signals ($\Delta F/F_0$ dendrite). Individual spine ROIs were then drawn to capture spine-specific fluorescence changes ($\Delta F/F_0$ spine). Due to the 100-fold volume difference between dendritic shafts and spines, backpropagating action potential (BAP)-related Ca^{2+} signals from the dendritic shaft typically invaded and dominated the Ca^{2+} signals measured in spines. To isolate genuine spine-specific Ca^{2+} transients, we implemented a three-step subtraction method. First, we plotted raw $\Delta F/F_0$ spine against $\Delta F/F_0$ dendrite for each spine-dendrite pair, which revealed two distinct signal components: a BAP-related component that scaled linearly with dendritic signals, and a spine-specific component independent of dendritic activity. Second, we removed the BAP-related component by subtracting a scaled version of the dendritic shaft signal from each spine signal, where $\Delta F/F_0$ spine specific = $\Delta F/F_0$ spine $- \alpha \times \Delta F/F_0$ dendrite. The scaling factor α was determined for each spine using robust regression (MATLAB function robustfit.m), which provided the slope of the linear relationship between spine and dendrite signals while minimizing the influence of outliers (Figure 2A and B). Third, following BAP signal removal, we assessed responsiveness of individual spines during motor movements, defining responsive spines as those exhibiting $\Delta F/F_0$ spine specific > threshold activity (mean plus two times standard deviation) for at least 10 consecutive frames.

Concurrently, we obtained behavioral data to extract running speed, timepoints, and durations of running epochs (REs) and stationary epochs (SEs).

Dendrites and synapses were determined 'active' by the presence of Ca^{2+} transients or events, which are fluorescent traces exceeding the threshold activity for a certain duration. Initial application of previously established definitions of Ca^{2+} transients (Yang et al., 2022) for Ca^{2+} events, which defined activity as fluorescence traces exceeding the mean plus three standard deviations of baseline fluorescence for at least three consecutive frames, resulted in the detection of both genuine Ca^{2+} activity and spurious fluorescent traces during periods of neuronal inactivity. The baseline fluorescence in the original method was calculated using $\Delta F/F_0$ values within the lower 50% of sorted fluorescence values for each ROI within an imaging session.

Given the inclusion of both noise and Ca^{2+} fluorescent activity when using this threshold for dendritic and synaptic Ca^{2+} activity, we systematically refined the criteria for Ca^{2+} transient detection through empirical evaluation of different threshold parameters. We tested various combinations of standard deviation multiples (2 and 3 STD, data not shown), and minimum duration requirements (3, 5, and 10 consecutive frames, data not shown). Optimal detection was achieved when fluorescence traces exceeded two standard deviations above the mean baseline fluorescence and persisted for a minimum of 10 consecutive imaging frames. The baseline for each ROI was calculated as the mean of all $\Delta F/F_0$ values during quiescent periods, identified as epochs with minimal fluorescence fluctuations. The first frame exceeding this threshold was defined as the onset of the Ca^{2+} event, while the event terminated when fluorescence dropped below threshold.

This refined definition effectively captured genuine Ca^{2+} transients in both dendrites and spines while excluding background noise signals and motion artifacts (Figure 2C and D). We

validated all detected events manually by cross-referencing with the corresponding Ca^{2+} imaging movies on a frame-by-frame basis, ensuring that identified transients corresponded to visible increases in fluorescence intensity rather than imaging artifacts or drift in baseline fluorescence. This validation step confirmed that the modified threshold parameters appropriately distinguished between true biological signals and technical noise in the two-photon imaging data.

Task-Correlated Dendritic and Synaptic Dynamics

To elucidate learning-associated changes in dendritic activity, we quantified the total number of Ca^{2+} transient events per minute in each dendrite throughout the training period. For this analysis, dendritic Ca^{2+} events were identified using the established criteria (fluorescence exceeding two standard deviations above baseline for at least 10 consecutive frames), then counted within each one-minute bin of the imaging session. The event frequency for each dendrite was calculated by averaging these per-minute counts across the entire recording session. Initial analysis pooling all dendrites revealed no significant differences in event frequency between early and late training phases (Figure 3B). However, this aggregate analysis potentially masked heterogeneous responses within the SST-IN population.

Previous work from the laboratory identified functionally distinct subpopulations of SST-INs in M1, distinguished by their expression of the activity-dependent immediate early gene NPAS4: task-responsive $NPAS4^{+}$ SST-INs that are selectively activated during learned motor behaviors, and task-irrelevant $NPAS4^{-}$ SST-INs that show no specific task-related modulation (Yang et al., 2022). To determine whether the imaged neurons belonged to these distinct functional classes, we performed post-hoc immunohistochemical staining in one experimental animal. This analysis revealed co-localization of GCaMP6s fluorescence with NPAS4

expression, confirming that the imaging captured both NPAS4^{+} and NPAS4^{-} SST-IN subpopulations (Figure 3A).

Based on this molecular evidence for functional heterogeneity, we re-analyzed the imaging data by categorizing neurons according to their predominant trajectory of dendritic activity change across training sessions (Figure 3C). This approach resulted in two distinct populations with opposing learning-related dynamics: 'positive neurons' that progressively increased their dendritic event frequency throughout training, and 'negative neurons' that showed progressive decreases in event frequency. This bidirectional modulation of dendritic activity aligns with the functional dichotomy between task-engaged and task-suppressed SST-IN subpopulations previously identified in motor learning contexts.

Analysis of Ca^{2+}imaging data revealed heterogeneous patterns of synaptic activity with varying degrees of temporal coordination with dendritic Ca^{2+} transients. Motor learning in M1 is known to involve dendritic Ca^{2+} spikes that drive potentiation of task-relevant spines through synchronized pre- and postsynaptic activity. In contrast, synaptic Ca^{2+} transients occurring independently of dendritic activity likely reflect spontaneous presynaptic glutamate release, which can regulate local spine dynamics through distinct plasticity mechanisms, including proBDNF/p75NTR-mediated synaptic depression. To systematically characterize these distinct modes of synaptic activity, we classified spine Ca^{2+} events based on their temporal relationship with dendritic transients. Independent spine events were operationally defined as those exhibiting less than 20% temporal overlap with concurrent dendritic Ca^{2+} events (Figure 3E), capturing synaptic activity driven primarily by presynaptic release. Conversely, co-active events were defined as those demonstrating greater than 80% temporal coincidence with dendritic Ca^{2+} transients (Figure 3D), representing synchronized pre- and postsynaptic activity. While these

temporal thresholds were selected empirically rather than derived from biophysical constraints, they effectively segregated spine events into functionally distinct categories. To assess learning-related changes in synaptic dynamics, we quantified the frequency of both independent and co-active spine events during early learning (naïve stage: training days 1-3) and following skill acquisition (expert stage: training days 10-12). Event frequencies were calculated for individual spines and subsequently averaged across all spines within each dendrite, then aggregated by neuron category to reveal population-level changes in synaptic activity patterns associated with motor learning.

To determine whether changes in dendritic activity patterns were associated with alterations in synaptic dynamics, we analyzed the proportion of spines showing increased coactive or independent events across training. Surprisingly, both positive neurons (those with increased dendritic activity) and negative neurons (those with decreased dendritic activity) exhibited similar proportions of spines with enhanced coactive events from early to late training (positive neurons: mean = 0.48, negative neurons: mean = 0.57, Mann-Whitney U test, $p = 0.3928$, n = 6 positive neurons, n = 7 negative neurons, Figure 4A). Similarly, the proportion of spines showing increased independent events did not differ between neuron categories (positive neurons: mean = 0.51, negative neurons: mean = 0.42, Mann-Whitney U test, $p = 0.9779$, Figure 4B). These findings indicate that changes in overall dendritic activity levels do not predict the direction of synaptic plasticity at individual spines. Examination of individual neurons revealed considerable heterogeneity within each category. Among positive neurons, the proportion of spines with increased coactive events ranged from 0.12 to 0.92, with neurons 2 and 6 showing the highest proportions (Figure 4C). Similarly, negative neurons displayed a wide range (0.20 to 0.88), with neuron 10 exhibiting the highest proportion (Figure 4C). This variability was also

evident in the proportion of spines with increased independent events (Figure 4D), suggesting neuron-specific plasticity patterns that transcend the simple positive/negative categorization.

Further analysis of spine coactivity during running specifically revealed that the mean number of running epoch (RE) coactive events per spine remained comparable between positive and negative neurons. During early training, positive neurons averaged 0.82 RE-coactive events per spine, while negative neurons showed 0.20 events (Mann-Whitney U test , $p = 0.9827$, Figure 4E). This pattern persisted in late training, with positive neurons maintaining 0.82 events and negative neurons showing 0.51 events (Mann-Whitney U test, $p = 0.9048$, Figure 4F). Neither neuron category showed significant changes in RE-coactivity levels across training phases (positive neurons: Mann-Whitney U test, $p = 0.9827$; negative neurons: Mann-Whitney U test, $p = 0.9048$). Individual neuron analysis revealed striking heterogeneity in RE-coactive event counts within both populations. Positive neurons showed particularly high variability, with neurons 2 and 4 exhibiting over 80 mean spine RE coactive events, while neurons 5 and 6 showed minimal coactivity (<10 events) (Figure 4G). Negative neurons displayed more moderate but still variable RE coactive event counts, ranging from approximately 10 to 60 events per spine (Figure 4H). This neuron-to-neuron variability suggests that motor learning engages diverse synaptic plasticity strategies even within functionally similar SST-IN subpopulations. These results demonstrate that synaptic plasticity mechanisms operate independently of global changes in dendritic activity. Despite opposing trends in dendritic Ca^{2+} event frequencies between positive and negative neurons, both populations maintained similar capacities for activity-dependent synaptic modification. The substantial heterogeneity observed at the single-neuron level further suggests that local synaptic plasticity rules, rather than cell-wide activity levels, govern the strengthening or weakening of individual synaptic inputs during motor learning.

To investigate the relationship between dendritic activity patterns and synaptic plasticity during running activity, we analyzed the proportion of spine coactive events relative to total dendritic events during running epochs (RE). This ratio revealed striking differences between positive and negative neuron populations that emerged with training. In positive neurons (those with increased dendritic activity across training), the distribution of spine RE coactive counts normalized to dendrite RE counts showed a significant leftward shift from early to late training phases (Kolmogorov-Smirnov (KS) test, $p < 0.001$) (Figure 5A). This indicates that despite increased overall dendritic activity in these neurons, the relative proportion of spine-dendrite coactivity during running decreased. Conversely, negative neurons (those with decreased dendritic activity) exhibited a rightward shift in this distribution (KS test, $p < 0.001$), demonstrating that the proportion of coactive events relative to total dendritic events increased during late training, even as overall dendritic activity declined (Figure 5B).

To determine whether initial spine-dendrite coupling during running could predict subsequent learning-related changes, we examined the relationship between the early-phase ratio of spine RE coactive events to dendrite RE events and the change in total spine event counts from early to late training. Linear regression analysis revealed only a weak negative correlation ($r = -0.3480$, $R^2 = 0.1216$, $p = 4.4515e-14$), with the regression equation: $y = -350.4317x + 4.0082$ (Figure 5C). This weak correlation coefficient ($|r| < 0.4$) indicates that the initial degree of spine-dendrite synchronization during locomotion is not a strong predictor of subsequent spine-specific plasticity.

These findings suggest that learning-induced changes in synaptic strength operate through mechanisms that are partially decoupled from global dendritic activity patterns. While positive neurons increase their overall dendritic Ca^{2+} transients, individual spines within these

neurons show reduced relative coupling to dendritic activity. Conversely, spines in negative neurons maintain or enhance their coupling to dendritic signals despite reduced global activity, potentially representing a compensatory mechanism to maintain synaptic efficacy in the face of decreased postsynaptic excitation.

To examine how dendritic-synaptic coactivity during running activity influences synaptic plasticity, we categorized spines based on their trajectory of coactive events during running epochs (RE) across training. Using cumulative distribution functions (CDFs), spines were classified into three groups based on their RE coactive event counts: (1) high-to-high spines, maintaining counts within the top 75th percentile in both early (days 1-3) and late training (days 10-12); (2) low-to-high spines, transitioning from the bottom 25th percentile to the top 75th percentile; and (3) high-to-low spines, shifting from the top 75th to bottom 25th percentile over the training period.

Analysis of calcium transient peak amplitudes, extracted as maximum $\Delta F/F_0$ values within each event and normalized to the standard deviation of all peak amplitudes, revealed striking bidirectional changes between coactive and independent synaptic events. For high-to-high spines, the distribution of peak amplitudes for coactive events significantly shifted rightward from early to late training (Kolmogorov-Smirnov test, $p < 0.001$, Figure 6A), indicating strengthening of synchronized synaptic responses. Conversely, peak amplitudes of independent events in the same spines showed a leftward shift (KS test, $p < 0.001$, Figure 6B), suggesting weakening of non-synchronized synaptic activity. This opposing pattern persisted across spine categories: low-to-high spines similarly exhibited increased coactive event amplitudes (KS test, $p < 0.001$, Figure 6C) paired with decreased independent event amplitudes (KS test, $p = 0.001$, Figure 6D) during late training. Even high-to-low spines, despite reducing

their coactive event frequency, maintained this inverse relationship between coactive and independent event amplitudes (KS test, $p < 0.001$ for both comparisons, Figure 6E and F).

When analyzing the pooled spine population, this bidirectional modulation remained robust, with coactive events showing significantly enhanced peak amplitudes (KS test, $p < 0.001$, Figure 6G) and independent events showing reduced amplitudes (KS test, $p < 0.001$, Figure 6H) following training. Importantly, this amplitude divergence was abolished when dendritic-synaptic coactivity was not properly identified (KS test, $p = 0.206$, Figure 6I), demonstrating that the temporal relationship between dendritic and synaptic activity is essential for driving these opposing plasticity changes. These results suggest that motor learning induces complementary strengthening of task-relevant synchronized inputs while suppressing non-synchronized synaptic activity, potentially enhancing signal-to-noise ratios in motor cortical circuits.

Summary

Two-photon Ca^{2+} imaging revealed distinct patterns of synaptic plasticity in SST-interneurons (SST-INs) during a 12-day motor learning task. SST-INs were classified into $NPAS4^{+}$ (task-responsive) and $NPAS4^{-}$ (task-irrelevant) populations based on dendritic activity trajectories. $NPAS4^{+}$ neurons exhibited increased dendritic activity but reduced relative spine-dendrite coactivity over training, suggesting a shift toward more selective synaptic integration. In contrast, $NPAS4^{-}$ neurons showed decreased dendritic activity but increased spine-dendrite coupling, possibly reflecting compensatory plasticity. Despite divergent dendritic activity, both neuron types displayed similar proportions of spines undergoing coactive and independent synaptic changes, highlighting the influence of local, rather than global, plasticity mechanisms.

To assess how dendritic-synaptic coactivity shapes these changes, spines were categorized into three subtypes based on their coactive event frequencies across training: *high-to-*

high (consistently high), *low-to-high* (increasing), and *high-to-low* (decreasing). All spine subtypes exhibited a robust bidirectional pattern, coactive event amplitudes increased, while independent event amplitudes decreased during late training, indicating activity-dependent refinement of synaptic inputs. This divergence persisted in the pooled spine population but was abolished when dendritic-spine coactivity was not considered, underscoring the critical role of synchronized activity. Together, these findings demonstrate that SST-INs undergo precise, coactivity-driven synaptic remodeling, enhancing task-relevant inputs and suppressing non-synchronous activity to optimize inhibitory circuit function during motor learning.

.

Discussion

This investigation elucidates novel mechanisms of input-driven dendritic and synaptic plasticity in SST-INs of M1 during motor skill acquisition. Through chronic in vivo two-photon calcium imaging in a head-fixed motor learning paradigm, we characterized dendritic and synaptic Ca^{2+} dynamics that potentially underlie motor expertise development. We identified two distinct SST-IN subpopulations defined by either increased or decreased dendritic events frequency across training sessions (designated positive and negative neurons, respectively). Post-hoc immunostaining revealed co-localization of GCaMP6s with $NPAS4^{+}$, suggesting these imaged neurons correspond to task-specific SST-INs previously characterized in M1. Quantification of spine-dendrite coactivity revealed a higher proportion of spines with increased coactivity in negative neurons compared to positive neurons. Critically, positive neurons exhibited higher spine-dendrite synchronization during running episodes in the early training phase compared to the late phase, while negative neurons displayed the opposite pattern. This temporal reorganization of synaptic activity indicates a shift from broad integration to selective refinement in positive neurons. The reduction in running-related co-activity in expert stages suggests increased specificity of dendritic-synaptic paired activity to specific motor actions, consistent with previous findings that SST-IN activity becomes more confined to specific motor tasks with learning. These results demonstrate that SST-INs optimize their circuit integration by maintaining a sparse but functionally relevant set of synaptic connections during motor skill acquisition, revealing cell-type specific mechanisms of inhibitory circuit plasticity.

Functionally Distinct Populations of SST-INs in Motor Learning

A key finding of our investigation is the identification of two functionally distinct populations of SST-INs based on their activity patterns across training: (1) positive neurons that

exhibited increased dendritic events and (2) negative neurons that showed decreased activity over the course of learning. This functional dichotomy aligns with our previous characterization of task-specific NPAS4^{+} and nonspecific NPAS4^{-} SST-IN subpopulations in M1, inspired by Yang et al., 2022. Post-hoc immunostaining results indicating GCaMP6s and NPAS4^{+} co-localization further supports the hypothesis that positive neurons represent the task-specific NPAS4^{+} SST-IN subtype. This distinction is significant as it demonstrates that inhibitory interneurons, traditionally regarded as a homogeneous population in circuit models, exhibit functional diversity that may serve different aspects of motor learning. These findings extend our understanding of interneuron diversity beyond the established molecular and morphological classifications (Kepecs & Fishell, 2014; Tremblay et al., 2016) to include functional specialization during learning. Such functional heterogeneity may allow for more precise regulation of excitatory-inhibitory balance during different phases of skill acquisition.

Temporal Dynamics of Spine-Dendrite Coupling

The most compelling aspect of our results is the divergent temporal patterns of spine-dendrite coupling observed in two neuronal populations. In positive neurons, spines demonstrated significantly higher synchronization with dendritic activity during the early phase of training compared to the late phase. This pattern suggests an initial period of broad synaptic integration followed by selective refinement as the animal develops expertise, consistent with a model of sparse but functionally relevant synaptic connections.

The observed reduction in running-related co-activity in the expert stage for positive neurons indicates increased specificity of dendritic-synaptic paired activity to particular motor actions. This temporal refinement mirrors findings in pyramidal neurons, where activity becomes sparser and more selective with learning (Peters et al., 2017; Komiyama et al., 2010). Our results

extend this principle to inhibitory circuits, suggesting that SST-INs undergo precise activity-dependent reorganization to optimize circuit integration during motor skill acquisition. Critically, our additional analyses of spine-level plasticity revealed a robust bidirectional modulation of calcium transient amplitudes depending on coactivity with dendritic events. By classifying spines into subtypes—high-to-high, low-to-high, and high-to-low—based on their frequency of coactive events during running epochs, we found that all groups exhibited increased peak amplitudes of coactive events and decreased amplitudes of independent events over training. This pattern was also present in the pooled spine population and was abolished when dendritic-synaptic coactivity was not accounted for. These findings suggest that the temporal coordination between spine and dendritic activity is not only a marker of synaptic relevance but a driving mechanism for plasticity. Such bidirectional changes likely reflect a learning-related sharpening of synaptic input selectivity, reinforcing task-relevant connections while weakening non-specific inputs.

Implications for Models of Inhibitory Circuit Plasticity

Our findings necessitate a reconsideration of current models of inhibitory circuit plasticity. The identification of functionally distinct SST-IN subpopulations with divergent patterns of synaptic reorganization during learning challenges conventional views of inhibitory neurons as a homogeneous population in circuit models. This functional heterogeneity aligns with the emerging understanding that inhibitory plasticity involves complex, codependent mechanisms essential for building nontrivial, functioning networks (Hennequin et al., 2017). The reduced co-activity observed in positive neurons during the expert stage aligns with previous work showing that SST-IN activity becomes more confined to specific motor tasks with learning (Adler et al., 2019). This increased specificity may serve to selectively suppress competing motor programs, thereby enhancing the execution of the learned behavior. Conversely, the

increased coupling in negative neurons during late-stage learning may function to maintain network stability as task-specific circuits are strengthened.

The bidirectional spine-specific plasticity observed across spine subtypes provides a mechanistic explanation for how these cell-type-specific changes emerge. The consistent strengthening of coactive inputs and suppression of independent events suggests that inhibitory circuits, like their excitatory counterparts, utilize spike-timing or coactivity-based rules to enhance signal-to-noise ratios during learning. Our findings support models where inhibitory circuits progressively refine to maintain precise excitatory-inhibitory balance (Vogels et al., 2011; Hennequin et al., 2017), potentially through the formation of negative feedback loops that dynamically stabilize task-specific excitatory assemblies (Murphy & Miller, 2009; Hennequin et al., 2014). The cell-type specificity we observed further suggests that different interneuron populations may contribute distinctly to what Hennequin et al. (2017) describe as "negative feedback control" in neural circuits, with some subpopulations potentially specializing in contextual gating or stimulus relay functions as learning progresses.

Methodological Advances and Limitations

Our study introduces several methodological advances for investigating inhibitory circuit plasticity. The head-fixed paradigm provides a simple model for studying learning-induced plasticity without confounding motivational factors. Additionally, our approach for isolating spine-specific calcium signals by subtracting dendritic contributions represents a significant technical improvement for studying synaptic dynamics in small neuronal compartments. Nevertheless, several limitations are taken into consideration. First, while our post-hoc immunostaining suggests correspondence between positive neurons and NPAS4^{+} SST-INs, more extensive molecular characterization would strengthen this association, as imaged neurons were

tentatively identified during post-hoc imaging. Second, our analysis focused on a relatively short imaging period: one from naïve and one from expert stage, to prevent photobleaching; longer imaging intervals might reveal additional phases of synaptic reorganization during consolidation and maintenance of motor skills. Finally, simultaneous recording of presynaptic inputs would provide valuable information about the sources of synaptic activity driving the observed plasticity, which opens more interesting questions.

Future Directions and Broader Implications

Future investigations should aim to identify the precise presynaptic partners of the differentially regulated synapses on SST-INs. Combining our imaging approach with optogenetic identification of specific input sources would illuminate how different circuit elements contribute to inhibitory neuron plasticity during learning. Additionally, examining how these patterns of inhibitory plasticity are altered in pathological conditions associated with motor learning deficits, such as Parkinson's disease or dystonia, could provide insights into disease mechanisms and potential therapeutic targets.

From a broader perspective, our findings suggest that inhibitory circuit plasticity may be as complex and nuanced as that observed in excitatory neurons, challenging simplistic models of interneuron function. The cell-type specificity and temporal dynamics we observed may be generalizable to other brain regions and learning contexts, suggesting a fundamental principle of inhibitory circuit organization.

In conclusion, our study reveals that SST-INs in M1 undergo precise, cell-type specific synaptic reorganization during motor learning, characterized by distinct temporal patterns of spine-dendrite coupling. These findings advance our understanding of inhibitory circuit plasticity

and provide a framework for investigating how inhibitory neurons contribute to learning and memory processes in the mammalian brain.

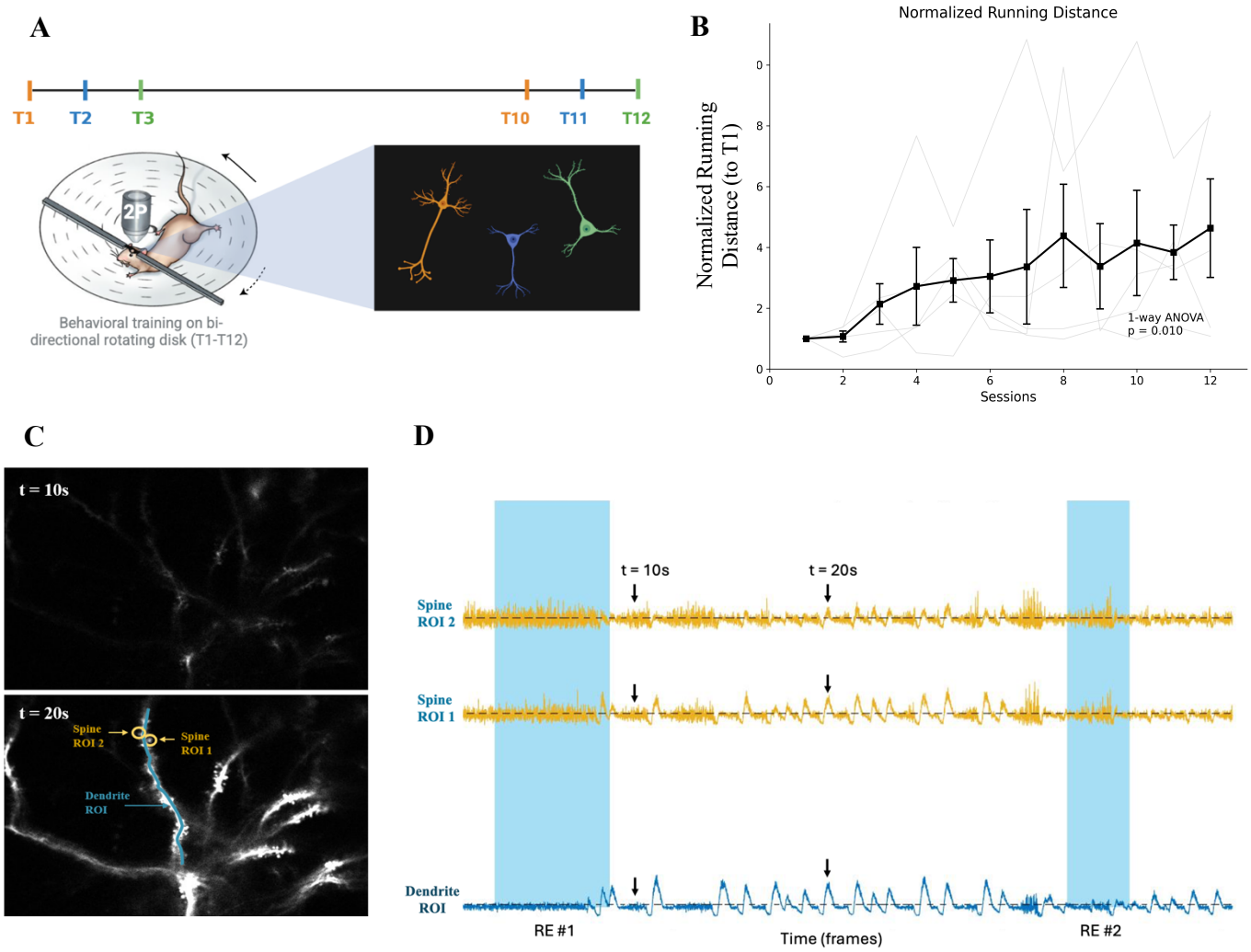

Figure 1: ***Dendritic and synaptic dynamics of L2/3 SST-INs in M1 during bi-directional running disk task in awake mice.*** **A.** Mice underwent 12-day training paradigm on bi-directional disk, individual neurons were imaged in rotation (neuron 1→2→3) during both early (days 1-3) and late (days 10-12) phases of the training paradigm. **B.** Total distance ran was normalized to the first day of training and averaged across all mice (blue). **C.** Time-lapse images during 10s and 20s and **D.** raw fluorescent traces of a representative dendritic branch (blue) and spines (yellow) selected as regions of interests (ROIs) capturing the time-lapsed image.

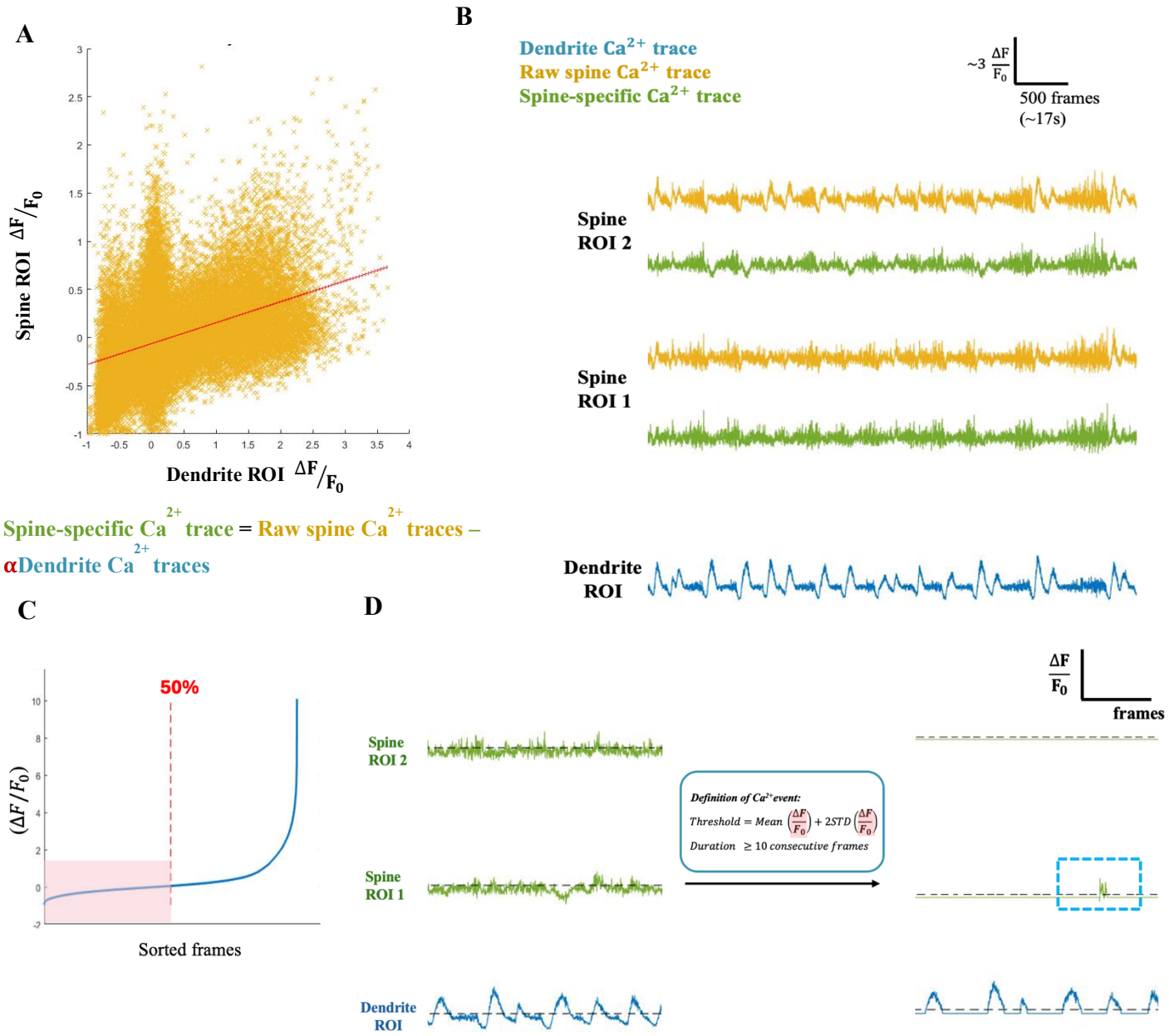

Figure 2: ***Characterization of dendritic and synaptic Ca^{2+} events.*** **A**. Removal of dendritic component in spine Ca^{2+} signals using an estimated contribution from robust linear fit of spine Ca^{2+} signals as a function of dendritic traces (Chen et al., 2013). **B.** Fluorescent traces of dendrite, spines before (yellow) and after (green) dendritic contribution removal. **C.** Sorted $\Delta F/F_0$ of each region of interest (ROI). **D.** Fluorescent traces of representative dendritic branch and spine ROIs that was identified as an event (blue box) using the determined threshold (above

mean and 2 STD of first half of sorted $\Delta F/F_0$ for at least 10 consecutive frames) from imaging data. Otherwise, $\Delta F/F_0$ is zeroed for illustration.

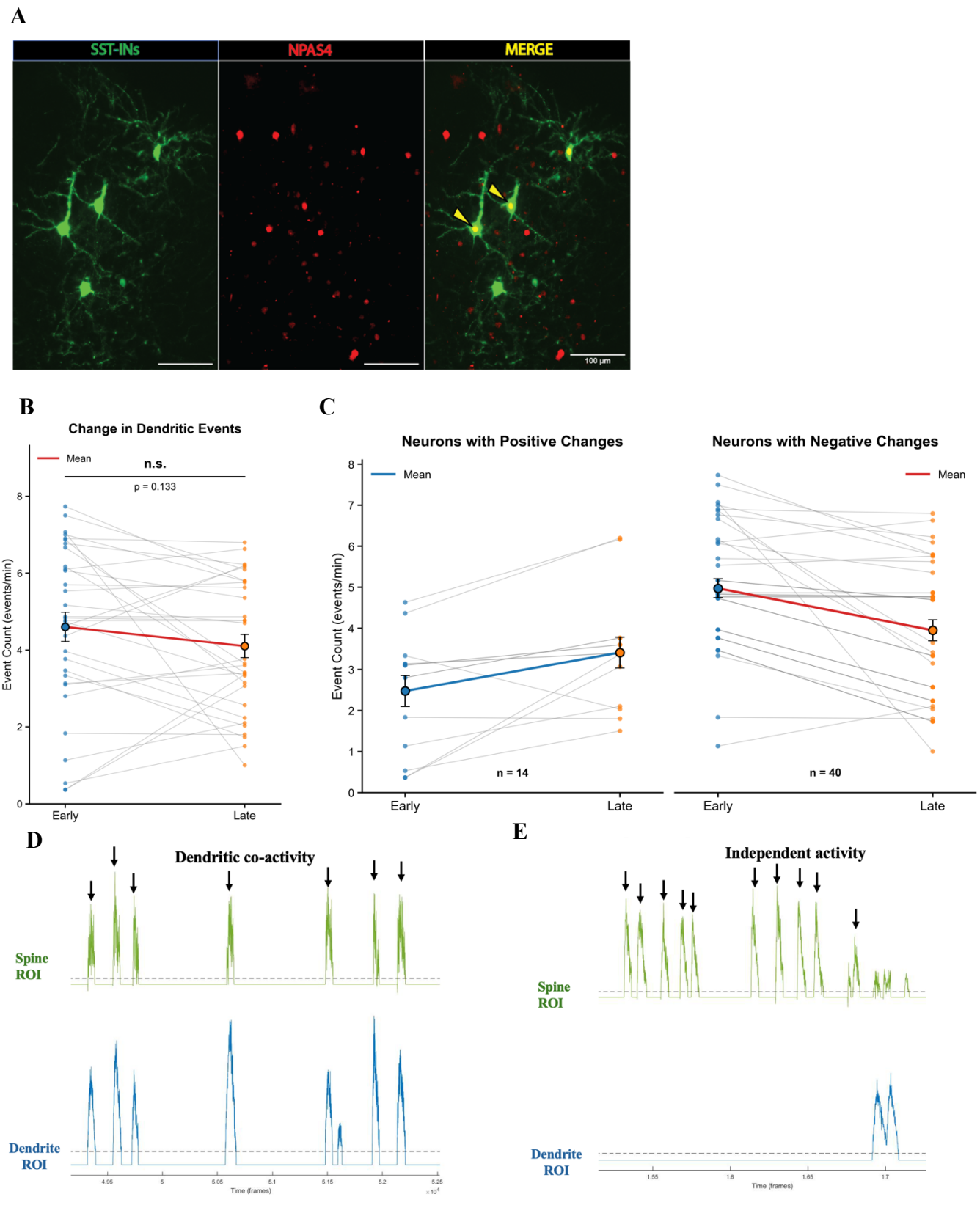
A
SST-INs
NPAS4
MERGE
100 µm
B
Change in Dendritic Events
Mean
n.s.
p = 0.133
Event Count (events/min)
Early
Late
C
Neurons with Positive Changes
Mean
Event Count (events/min)
n = 14
Early
Late
Neurons with Negative Changes
Mean
n = 40
Early
Late
D
Dendritic co-activity
Spine ROI
Dendrite ROI
Time (frames)
E
Independent activity
Spine ROI
Dendrite ROI
Time (frames)

Figure 3: ***Activity-dependent classification of SST-INs reveals distinct subpopulations during motor learning.*** **A.** Post-hoc immunohistochemical verification of NPAS4 expression in putative imaged neurons. **B.** Changes in dendritic calcium event frequency across motor learning. Individual dendrites (n=54) are shown with gray lines connecting early (days 1-3) and late (days 10-12) training phases. Blue dots represent early training values, orange dots represent late training values. Large circles with error bars show population means ± SEM. Red line indicates mean trajectory. No significant difference was observed at the population level (paired t-test, p=0.133, n.s.). **C.** Categorization of neurons based on dendritic activity trajectories reveals opposing plasticity patterns. Left panel: Positive neurons (n=14 dendrites from 6 neurons) showing increased dendritic event frequency from early to late training. Blue line indicates mean trajectory with significant increase (mean ± SEM: 2.50 ± 0.32 to 3.47 ± 0.27 events/min). Right panel: Negative neurons (n=40 dendrites from 7 neurons) showing decreased dendritic event frequency. Red line indicates mean trajectory with significant decrease (mean ± SEM: 4.96 ± 0.20 to 3.97 ± 0.29 events/min). Individual dendrite trajectories shown in gray demonstrate considerable heterogeneity within each population, with some dendrites showing changes opposite to their group's mean trend. This bidirectional modulation supports the existence of functionally distinct SST-IN subpopulations that are differentially engaged during motor learning. **D.** Dendritic-synaptic coactive (i.e. coactivity) events are synaptic events with more than 80% overlapping with respective parent dendrite. **E.** Independent synaptic events are spine events with less than 20% overlapping with respective parent dendrite.

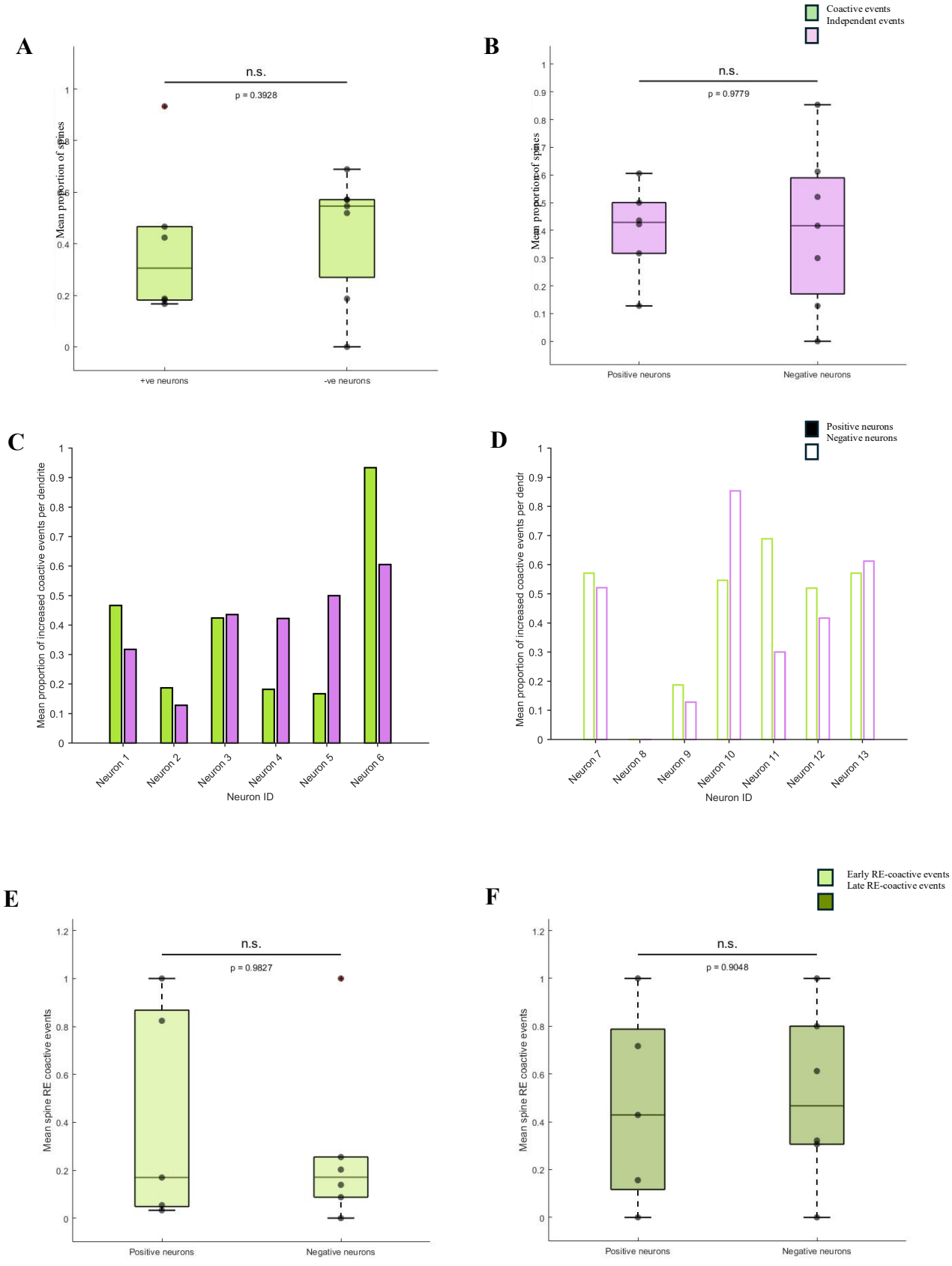
A
n.s.
p = 0.3928
Mean proportion of spines
+ve neurons
-ve neurons
B
Coactive events
Independent events
n.s.
p = 0.9779
Mean proportion of spines
Positive neurons
Negative neurons
C
Mean proportion of increased coactive events per dendrite
Neuron 1
Neuron 2
Neuron 3
Neuron 4
Neuron 5
Neuron 6
Neuron ID
D
Positive neurons
Negative neurons
Mean proportion of increased coactive events per dendr
Neuron 7
Neuron 8
Neuron 9
Neuron 10
Neuron 11
Neuron 12
Neuron 13
Neuron ID
E
n.s.
p = 0.9827
Mean spine RE coactive events
Positive neurons
Negative neurons
F
Early RE-coactive events
Late RE-coactive events
n.s.
p = 0.9048
Mean spine RE coactive events
Positive neurons
Negative neurons

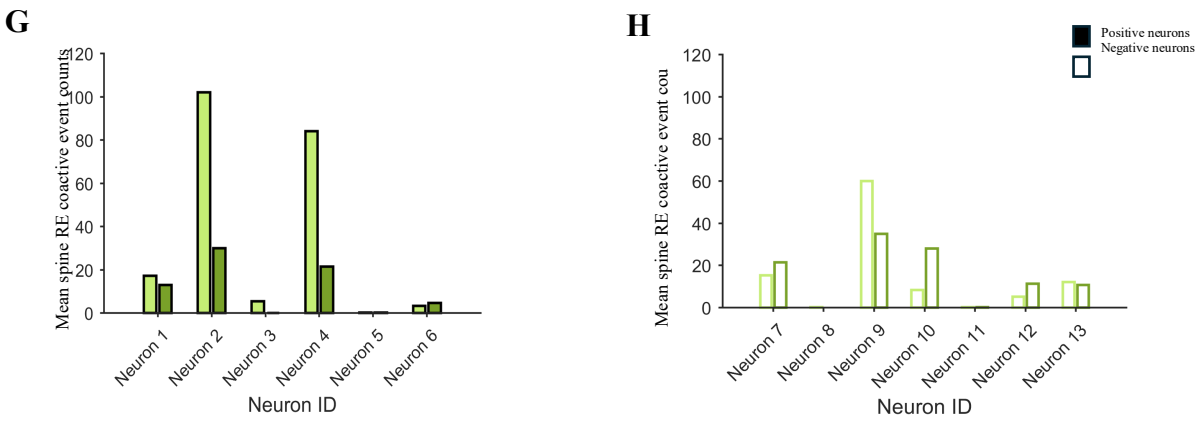

Figure 4. ***Analysis of spine event proportions and RE-coactive events across neuron categories.*** **A.** and **B.** Proportion of spines with increased coactive and independent events between positive and negative neurons. **A.** Box plots showing the mean proportion of spines per dendrite with increased coactive events from early (days 1-3) to late training (days 10-12) for positive neurons (green, n=6) and negative neurons (dark green, n=7). No significant difference was observed between groups (p=0.3928, Mann-Whitney U test). **B.** Box plots showing the mean proportion of spines per dendrite with increased independent events for positive neurons (light purple) and negative neurons (dark purple). No significant difference was observed between groups (p=0.9779, Mann-Whitney U test). Box plots show median (central line), interquartile range (box), and individual neuron data points. **C.** Bar graph showing the proportion of spines with increased coactive events (green) and independent events (pink) for each positive neuron (Neurons 1-6). **D.** Bar graph showing the same measures for negative neurons (Neurons 7-13). Individual neurons display considerable heterogeneity within each category, with proportions ranging from 0.12 to 0.92 for coactive events and 0.11 to 0.88 for independent events. **E.** Box plots comparing RE-coactive event counts during early phase between positive and negative neurons (p=0.9827, Mann-Whitney U test). **F.** Box plots comparing RE-coactive event counts during late phase between groups (p=0.9048). Light green bars represent early training, dark

green bars represent late training. Neither group showed significant changes across training (positive neurons: p=0.9827, Mann-Whitney U test; negative neurons: p=0.9048, Mann-Whitney U test). **G.** Bar graph showing early (light green) and late (dark green) training RE-coactive event counts for each positive neuron. Neurons 2 and 4 show particularly high coactivity (>80 events), while neurons 5 and 6 show minimal coactivity (<10 events). **H.** Same analysis for negative neurons, showing more moderate RE-coactive event counts ranging from approximately 10 to 60 events per spine.

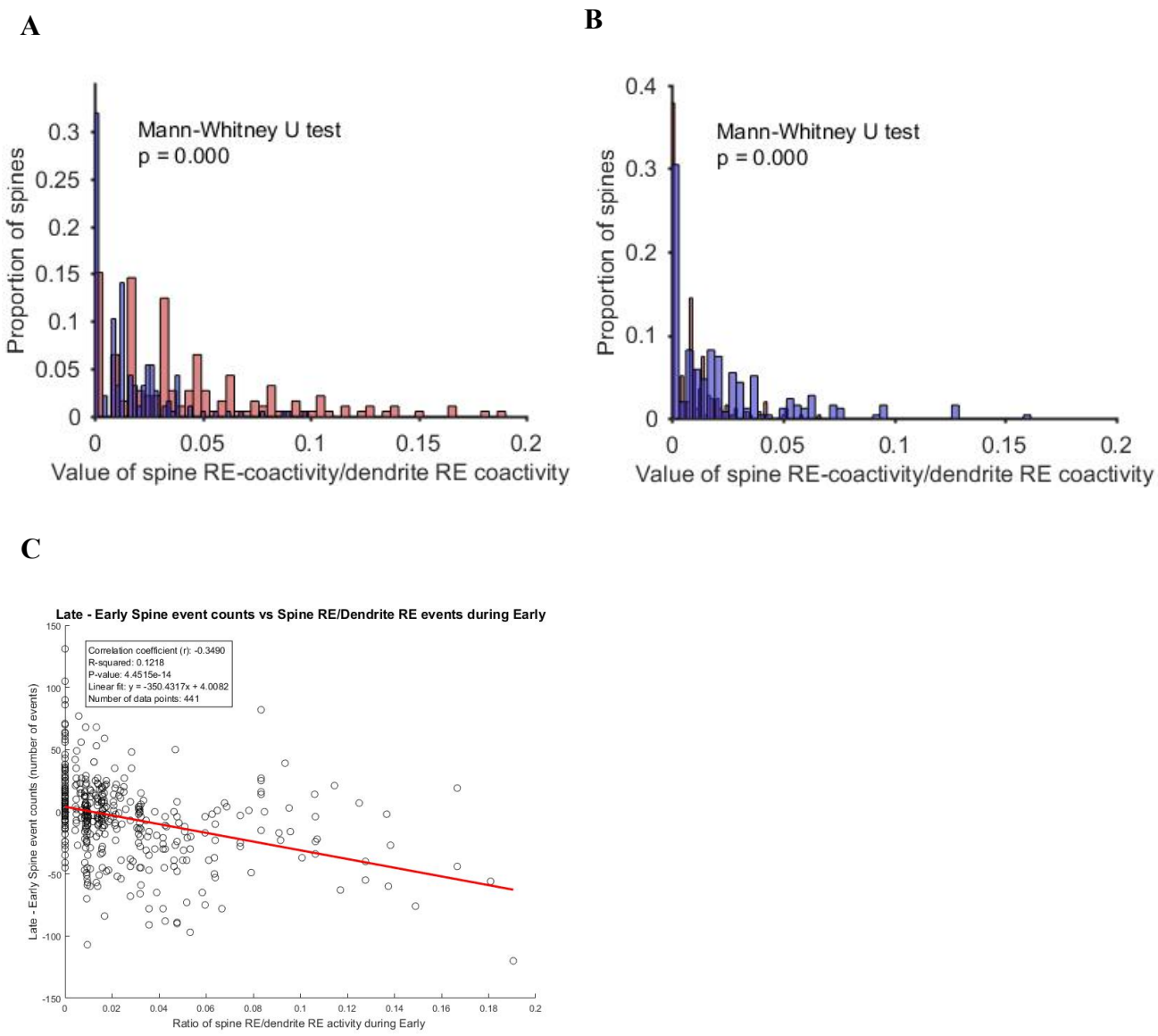

Figure 5. ***Dendritic activity influences on spine-dendrite coupling during running activity.*** **A.** Histogram showing the distribution for positive neurons during early (red) and late (blue) training. The distribution significantly shifts leftward from early to late training (Kolmogorov-Smirnov test, $p<0.001$), indicating reduced relative spine-dendrite coupling despite increased overall dendritic activity. **B.** Histogram for negative neurons showing a rightward shift from early to late training (KS test, $p<0.001$), demonstrating increased relative coupling as dendritic activity decreases. Y-axis shows proportion of spines, X-axis shows the ratio of spine RE-

coactive counts to dendrite RE counts. **C.** Correlation analysis between early-phase spine-dendrite coupling and subsequent changes in spine activity. Scatter plot showing the relationship between the ratio of spine RE-coactive events to dendrite RE events during early training (x-axis) and the change in total spine event counts from early to late training (y-axis). Each point represents an individual spine (n=441 spines). Red line shows linear regression fit ($y = -350.4317x + 4.0082$, $r = -0.3480$, $R^2 = 0.1216$, $p = 4.4515e-14$). The weak correlation coefficient ($|r| < 0.4$) indicates that initial spine-dendrite synchronization during locomotion is not a strong predictor of learning-related synaptic plasticity.

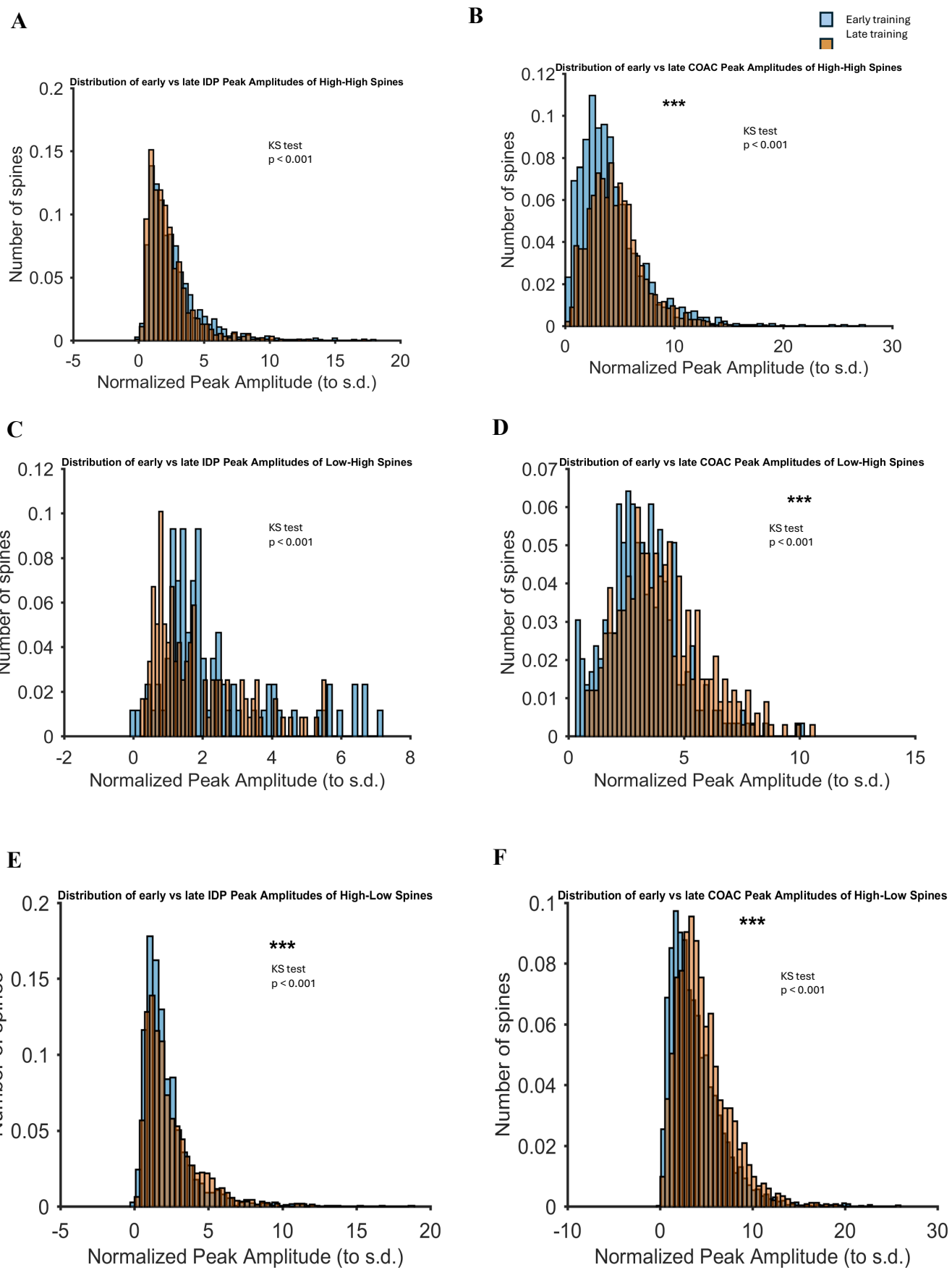
A
Distribution of early vs late IDP Peak Amplitudes of High-High Spines
KS test
p < 0.001
Number of spines
Normalized Peak Amplitude (to s.d.)
B
Early training
Late training
Distribution of early vs late COAC Peak Amplitudes of High-High Spines
***
KS test
p < 0.001
Number of spines
Normalized Peak Amplitude (to s.d.)
C
Distribution of early vs late IDP Peak Amplitudes of Low-High Spines
KS test
p < 0.001
Number of spines
Normalized Peak Amplitude (to s.d.)
D
Distribution of early vs late COAC Peak Amplitudes of Low-High Spines
***
KS test
p < 0.001
Number of spines
Normalized Peak Amplitude (to s.d.)
E
Distribution of early vs late IDP Peak Amplitudes of High-Low Spines
***
KS test
p < 0.001
Number of spines
Normalized Peak Amplitude (to s.d.)
F
Distribution of early vs late COAC Peak Amplitudes of High-Low Spines
***
KS test
p < 0.001
Number of spines
Normalized Peak Amplitude (to s.d.)

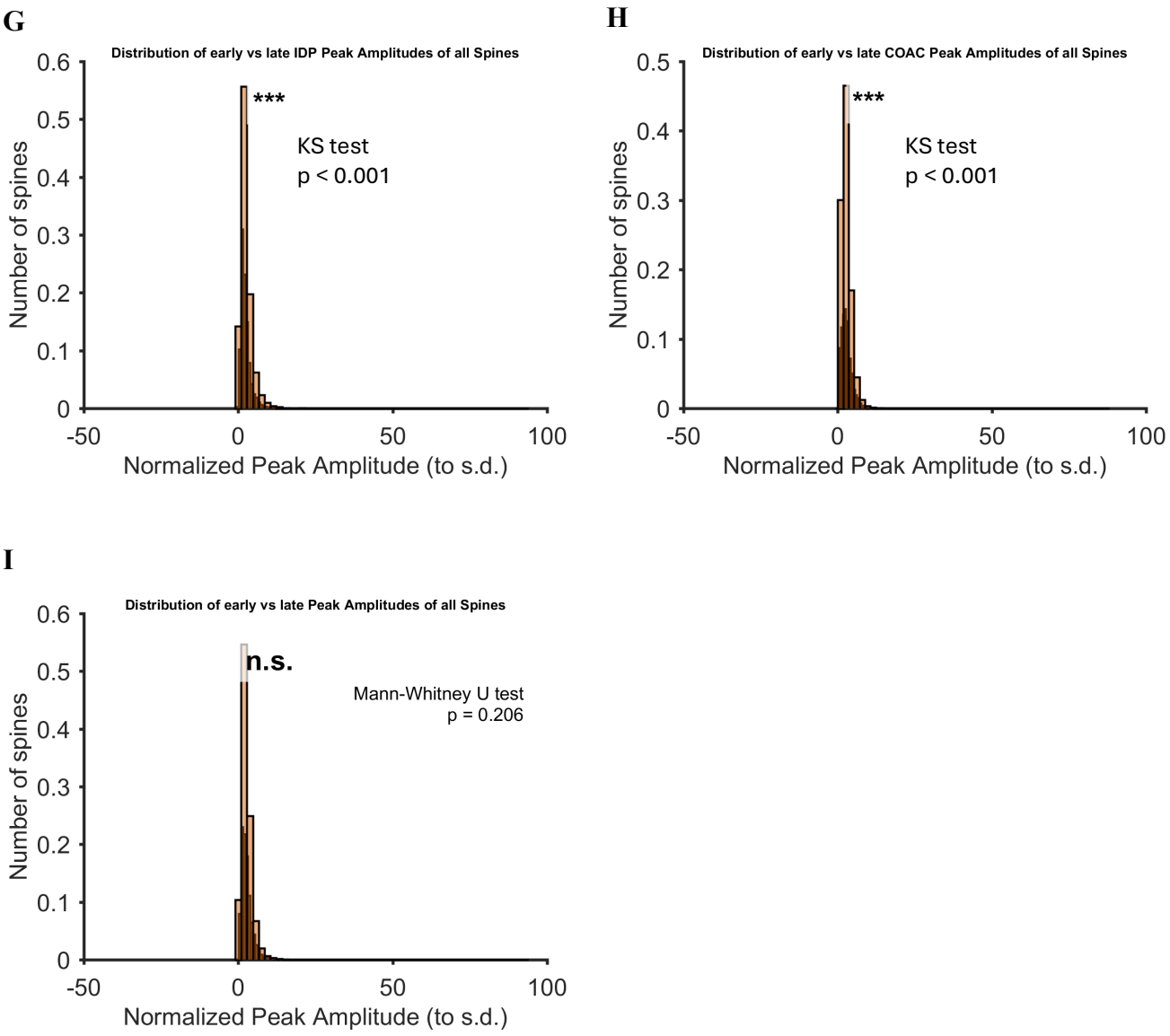

Figure 6. ***Bidirectional modulation of synaptic event amplitudes driven by dendritic-synaptic coactivity during motor learning*****. A-F:** Spine-level analysis of calcium transient peak amplitudes ($\Delta F/F_0$) in three categories of dendritic spines, classified based on the trajectory of their coactive event counts during running epochs (RE) across early (days 1–3) and late (days 10–12) training phases. **A-B.** High-to-high spines (top 75th percentile in both early and late RE coactivity): **A.** Distribution of coactive event amplitudes shifted rightward during late training (KS test, $p < 0.001$), indicating potentiation of synchronized synaptic inputs. **B.** Independent

event amplitudes decreased (leftward shift, KS test, $p < 0.001$), suggesting depression of non-coactive inputs. **C-D.** Low-to-high spines (bottom 25th to top 75th percentile RE coactivity): **C.** Coactive events showed increased amplitudes in late training (KS test, $p < 0.001$); **D.** Independent events showed decreased amplitudes (KS test, $p = 0.001$), reinforcing the inverse modulation. **E-F.** High-to-low spines (top 75th to bottom 25th percentile RE coactivity): Despite reduced coactivity frequency, the pattern persisted—coactive events increased in amplitude **E.** and independent events decreased **F.** (KS tests, $p < 0.001$ for both), indicating sustained bidirectional plasticity. **G-H.** Pooled analysis across all spines confirmed robust divergence in amplitude modulation: **G.** Coactive events increased in amplitude (KS test, $p < 0.001$), and **H.** independent events decreased (KS test, $p < 0.001$) after training. **I.** When dendritic-synaptic coactivity was not specifically identified, this bidirectional amplitude modulation was abolished (KS test, $p = 0.206$), underscoring the importance of dendritic-spine synchrony in shaping synaptic plasticity.

Method Details:

Animals:

All animal experiments are approved by the University of Ottawa Animal Care Committee in accordance with the Canadian Council on Animal Care guidelines. Mice are group housed in plastic cages with food and water ad libitum in a room with a reversed light cycle (12h - 12h). For this experiment, the transgenic mouse line SST-IRES-Flp (Jackson Laboratory, Stock No. 031629) are used for cell-type specific sparse labelling of SST-INs. The colony of SST-IRES-Flp mice is generated by crossing male with female SST-IRES-Flp. All mice are bred in-house and housed in a 21–23 °C and 40–60% humidity facility with free access to food and water. Experimental mice are group-housed in plastic cages with food and water ad libitum in a room with a reversed light cycle (12 h/12 h).

Headplate implantation/Craniotomy surgery and virus injection:

Prior to the surgery, mice are subcutaneously injected with buprenorphine (0.05 mg/kg), Baytril (5 mg/kg), and Dexthamethasone (2 mg/kg) as analgesia, anti-infection, and anti-inflammation, respectively and anesthetized with 1-2% of isoflurane. An incision is performed to remove the scalp, which exposes the skull. The skull is scraped with blade scalpel to increase the skull surface area; a customized metal head plate or bar is implanted on the skull with glue (Krazy Glue). A craniotomy of approximately 2 mm in diameter is performed over the right forelimb motor cortex (M1; 300µm anterior and 1,500µm lateral from the bregma). A mixture of viruses (University of Pennsylvania Vector Core; Ca^{2+}imaging; AAV2/1-CAG-fDIO-Cre-P2A-mNeptune in 1: 5,000 dilution (in saline) and mixed with AAV1-Syn-Flex-GCaMP6s-WPRE-SV40 in 1:1 dilution) is injected at M1 at both 280µm and 300µm depth (2 sites, ~100 nl/site) from the pia. Each virus is injected over 5 min and the injecting glass pipette is maintained in the

brain for at least 5 min to prevent backflow. After virus injections, a glass window is implanted over M1, and the implants are stabilized with Jet Denture Repair Powder Cement (Henry Schein). Following surgery, mice are given buprenorphine (0.1mg/kg), and dexamethasone (2mg/kg) to prevent infection. Mice recover in home cage for 3 weeks before behavioral training and two-photon imaging.

Head-fixed bidirectional running disk task:

A 14cm diameter running disk is mounted on an axle containing an optical encoder (US digital) that is sensitive to rotational displacement of 0.018cm or more in either direction. The mouse is head-fixed 3cm from the disk center by the headplate attached from surgery. At 5 days before training/imaging sessions, mice are habituated daily to head fixation inside a plastic tube for 3 minutes. Each training session is 1h/day for 12 sessions, with total running distance and speed recorded. A running epoch (RE) is defined as when mice exceed and maintain the running velocity above the threshold for more than 3s. Mice are habituated to the spinning-disk environment for 3-5 days prior to the start of training. Habituation includes fixing the head of the mouse to the running disk stage for 3-5 minutes per day while the body of the mouse is held stationary in a plastic holding tube. After habituation, the training begins and takes place for 12 consecutive days, consisting of 60-minute sessions each day.

Chronic two photon dendrite and spine Ca^{2+} imaging:

For two-photon Ca^{2+} imaging, SST-Flp mice are injected with a mixture of viruses: AAV2/1-CAG-fDIO-Cre-P2A-mNeptune (University of Pennsylvania Vector Core; Ca^{2+}imaging; in 1: 5,000 dilution with saline) and AAV1-Syn-Flex-GCaMP6s-WPRE-SV40 (in 1:1 dilution). During the craniotomy surgery, the mixture is injected into L2/3 M1 (2 sites, 100 nl at each site) around the center of the window. Each injection is given at a depth of 280 and

300μm from the pia. 3 to 4 weeks later, dendrites and synapses of SST-INs are imaged using a commercial two-photon microscope (B-scope, Thorlabs) using a ×16 objective (NIKON) with excitation at 925 nm (InSight X3, Spectra-Physics) at 30 Hz. ScanImage implemented in MATLAB 2015 is used to record two-photon Ca^{2+} imaging data. Images are acquired on one plane at ~250 μm (L2/3) from pia for the first 30 minutes while mice are running on the rotating-disk. The same imaging plane is followed in the later session. Due to sparse labeling, I can choose the imaging field that has the brightest dendritic branches with easy-to-see spines of these dendrites, and ideally from identifiable individual parent somas. Two photon imaging is performed for three neurons over a 12-day training period, with 30-minute sessions conducted at the beginning of both early (T1-3) and late (T10-12) training phases. Each neuron is imaged in a rotating schedule across paired early-late sessions (neuron #1 on T1/T10, neuron #2 on T2/T11, and neuron #3 on T3/T12) (Figure 1A). Wavesurfer implemented in MATLAB 2015 is used to record running distance and calculate running velocity and duration per session and is synchronized with Scanimage using Yoke to WaveSurfer to ensure in-real time recording of learning-related dendritic and synaptic activity.

Data pre-processing:

Lateral motion of Ca^{2+} imaging data is corrected using full-frame cross-correlation image alignment (Turboreg plug-in ImageJ). A custom MATLAB program is used to manually draw regions of interest (ROIs) on dendritic shaft and spines that show clear and robust fluorescent activity, with reference to criteria in Chen et al., 2013 and Cichon and Gan, 2015. Dendritic shafts containing at least four clearly identifiable spines are selected for signal extraction. Large spines, likely mushroom spines, are preferentially selected due to their transparent signals, while small and dim spines are excluded from analysis due to low signal-to-noise ratio. Spine ROIs are

defined with deliberate exclusion of spine necks. Followingly, ROIs are aligned across sessions for monitoring across sessions using the recursive alignment of stacks of images (Stackreg, plug-in ImageJ) (Peters et al., 2014). Fluorescence traces for each ROI are generated by averaging pixels within the ROI. The baseline (F_0) fluorescence trace is approximated using a custom MATLAB program as described (Peters etal., 2014). Fluorescence change (ΔF) is yielded by subtracting F_0 from the raw trace and dividing by F_0 to obtain the standardize fluorescence trace values ($\Delta F/F_0$).

Two photon Ca^{2+} Imaging Analysis:

The baseline (F_0) of each ROI is calculated by averaging smoothed original fluorescence trace from the whole session (Peters et al., 2014). ΔF is yielded by subtracting F_0 from the raw fluorescence. Dendrites and synapses are determined 'active' when they maintain above the activity threshold for ten or more consecutive imaging frames, at least once throughout the imaging session (calculate independently for each ROI). The first frame is defined as the start of the Ca^{2+} event, and the end of the event is identified as three or more consecutive frames with a $\Delta F/F_0$ lower than the activity threshold. The activity threshold is calculated as the mean + 2x the standard deviation of the baseline fluorescence traces ($\Delta F/F_0$) values that are within the lower 50^{th} percentile of the sorted $\Delta F/F_0$ values for each ROI within an imaging session (Figure 2C and D).

To eliminate back-propagating action potential (BAP) Ca^{2+} signals that enter the observed spines, we employ robust linear regression to subtract dendritic contamination, as inspired by Chen et al., 2013. Initially, we define ROIs of parent dendritic shafts for each imaging session to measure the global BAP-related dendritic signal (dendrite $\Delta F/F_0$). Due to the dendritic shaft's volume being roughly 100 times larger than tuned dendritic spines, any

fluorescent traces from spines to dendrite $\Delta F/F_0$ is considered negligible, confirmed by principal component analysis (Chen et al., 2013). When plotting spine $\Delta F/F_0$ against dendrite $\Delta F/F_0$, we identify two distinct components in spine signals: a BAP-related component and a spine-specific component. Next, we remove the BAP-related component from spine signals by subtracting a scaled version of dendritic signal: spine-specific $\Delta F/F_0$ = raw spine $\Delta F/F_0 - \alpha$ x dendrite $\Delta F/F_0$ (Figure 2A). The scaling factor α is calculated using robust regression ('robustfit() function in MATLAB R2017a) of spine $\Delta F/F_0$versus dendrite $\Delta F/F_0$, represented by the slope of the robust fitted line in Figure 2A.

Inspired by Yang et al., we hypothesized that motor learning induces two functionally distinct groups of SST-INs: task-relevant NPAS4+ SST-INs and non-specific NPAS4- SST-INs. Previous work showed reduced neuronal activity NPAS4+ SST-INs, and thus, hypothesized to alleviate inhibition onto postsynaptic excitatory neurons. A potential indicator of neuronal activity is dendritic activity (Golding and Spruston, 2002; Kampa and Stuart, 2006; Remy and Spruston, 2007; Hotlhoff et al., 2004; Humeau and Luthi, 2007). Hence, we quantify the change in total number of dendritic events between early and late phase (change = late – early) and find two functional subgroups of imaged SST-INs: one with increased and one with decreased total number of dendritic event (termed ‘positive’ and ‘negative’ neurons, respectively). Notably, neurons with less than 5 dendritic events during both sessions are not included.

Dendritic-synaptic coactivity (i.e. coactive events) are synaptic events with at least 80% overlap in duration with their respective parent dendritic events (Figure 3C). In contrast, independent synaptic events (i.e. independent events) are synaptic events with less than 20% overlap in duration with their respective parent dendritic events (Figure 3D).

For Figure 4C and D, we quantify the proportion of spines with increased coactive events after motor training over total number of spines per dendritic branch, then average the obtained value across all branches of the same neuron to acquire the mean percentage of increased coactive synaptic events within each neuron. We repeat the same analysis for quantifying mean percent of increased independent synaptic events per neuron.

Then, we compare the averaged percent of increased coactive and independent spine events between positive and negative group. Past studies showed that dendrite-spine activity coincidence results in potentiation of said spine (Golding and Spruston, 2002; Kampa and Stuart, 2006; Remy and Spruston, 2007; Hotlhoff et al., 2004; Humeau and Luthi, 2007). Therefore, coactive events may be an indicator of potentiated synapses. By quantifying the mean proportion of increased coactive synaptic events across training, we can potentially infer overall level of potentiation at the neuronal level.

We then investigate the relation between coactivity during REs for individual neurons. We isolate and quantify coactive events with at least 80% overlap in duration with REs (i.e. RE-coactivity) per spine during early training phase. Then, we average this across all spines of the same parent dendrite, followed by averaging across all dendrites of the same neuron. We repeat the same analysis for coactive events during late phase and compare the mean counts of RE-coactivity between early and late phase for each animal, as well as between positive and negative neuron groups (Figure 4E and F).

For further investigation of how running-related dendritic activity impact synaptic events, we first isolate dendritic events and spine coactive events during RE by at least 80% overlap in duration (i.e. RE coactive events and RE dendritic events, respectively). Then, we quantify the counts of RE coactive events for each spine during the early phase and calculate the ratio of the

obtained value over the total number of RE dendritic events (parent dendrite). We standardize these ratios across spines within each neuron by normalizing values relative to the standard deviation of accumulated ratios of all spines of the same neuron, and pool the values for all spines to obtain the distributions of spine RE coactivity/dendrite RE activity of positive (Figure 5A) and negative (Figure 5B) neurons during the early phase. Repeating the same analysis for the late phase, we then compare the distributions of spine RE coactivity/dendrite RE activity between early and late phase within each subgroup using ranksum() function in MATLAB R2017.

Immunostaining:

Following training, brain sections of mice are collected around the M1 region for tentative detection of imaged SST-INs and characterization of NPAS4 expression. Brain sections around the Bregma are collected, where M1 is identified as 300μm anterior to the Bregma. Slices are washed 3 x 10 min in PBS, followed by permeabilization 3 x 10 min in PBS-T (PBS with 1% Triton X-100), and incubated for 2 hours in blocking solution (PBS-T with 10 % Normal Donkey Serum). Afterwards, slices are placed and incubated in primary antibody solution overnight at 4°C. The following primary antibodies are utilized in separate experiments: rabbit anti-NPAS4 (1:500, Activity Signaling, ASAB18A-100), chicken anti-GFP (1:2000, Milipore, MAB3120). The next day, brain sections are washed 5 x 10 min in PBS-T, incubated in secondary antibodies at room temperature for 2 hours. The following secondary antibodies are used for separate experiments: Alexa FluorÒ Plus 488 goat anti-rabbit (1:500, Invitrogen, A32731). After incubation, brain slices are washed 3 x 10 min in PB and mounted onto microscope slides with VECTASHIELD HardSet Mounting Medium with DAPI (VECTOR Laboratories, H-1200-10). All incubations are processed on a rocking shaker. Imaging is conducted using a Zeiss Axio

Imager 2 Microscope (M2), and putative imaged cells are identified based on GFP expression and morphological comparison with previously acquired two-photon Ca^{2+} imaging data.

Spine categorization based on running-related coactivity trajectories

To investigate activity-dependent synaptic plasticity during motor learning, spines were categorized based on their patterns of coactive events specifically during running epochs (RE) across training. For each spine, we quantified the number of coactive calcium events (>80% temporal overlap with dendritic transients) that occurred during running epochs in both early (days 1-3) and late (days 10-12) training phases.

Cumulative distribution functions (CDFs) were computed separately for early and late training phases using the RE coactive event counts from all spines. Spines were then classified into three categories based on percentile thresholds: (1) High-to-high spines: those with RE coactive event counts within the top 75th percentile during both early and late training phases; (2) Low-to-high spines: those transitioning from the bottom 25th percentile during early training to the top 75th percentile during late training; and (3) High-to-low spines: those shifting from the top 75th percentile during early training to the bottom 25th percentile during late training. The same categorization approach was applied independently for spines based on their independent event counts (<20% temporal overlap with dendritic transients) during running epochs.

Analysis of calcium transient peak amplitudes

To assess changes in synaptic strength, we analyzed the peak amplitudes of calcium transients for both coactive and independent events. For each detected calcium event in every spine, the peak amplitude was extracted as the maximum $\Delta F/F_0$ value occurring within the event

duration. Peak amplitudes were then pooled across all spines within each category (high-to-high, low-to-high, or high-to-low) separately for early and late training phases.

To enable comparison across different spines and imaging sessions, all peak amplitude values were normalized by dividing by the standard deviation of the entire peak amplitude distribution (pooled across all spines, events, and time points). Distribution histograms of these normalized peak amplitudes were generated for each spine category and event type (coactive or independent), comparing early versus late training phases. Statistical comparisons between distributions were performed using the Kolmogorov-Smirnov test to detect shifts in amplitude distributions indicative of synaptic strengthening or weakening.

Statistical Analyses:

All statistical analyses are performed using MATLAB R2017a. Statistical significance of changes in total running distance across 12 training days is determined via 1-way ANOVA with Bonferroni corrections. For quantification of changes in dendritic events, paired t-test is used. We use Mann-Whitney U test (ranksum() function in MATLAB) to verify statistical significance of the differences between change sin proportion of spines with increased coactive and independent events across training, and Kolmogorov–Smirnov test (kstest() in MATLAB) for distributions of spine RE coactivity/ dendrite RE activity in the early and late phase.

Disclaimers:

All immunostaining experiments are performed by Jan Rainer Sidiangco (PhD candidate, Simon Chen lab). I perform the rest of the experiments, including data collection and analyses.

References:

Adler, A., Zhao, R., Shin, M. E., Yasuda, R., & Gan, W. B. (2019). Somatostatin-Expressing Interneurons Enable and Maintain Learning-Dependent Sequential Activation of Pyramidal Neurons. *Neuron*, *102*(1), 202–216.e7. https://doi.org/10.1016/j.neuron.2019.01.036

Bloodgood, B., Sharma, N., Browne, H. *et al.* The activity-dependent transcription factor NPAS4 regulates domain-specific inhibition. *Nature* 503, 121–125 (2013). https://doi.org/10.1038/nature12743

Castillo, P. E., Chiu, C. Q., & Carroll, R. C. (2011). Long-term plasticity at inhibitory synapses. *Current opinion in neurobiology*, *21*(2), 328–338. https://doi.org/10.1016/j.conb.2011.01.006

Chen, S. X., Kim, A. N., Peters, A. J., & Komiyama, T. (2015). Subtype-specific plasticity of inhibitory circuits in motor cortex during motor learning. *Nature neuroscience*, *18*(8), 1109–1115. https://doi.org/10.1038/nn.4049

Chevaleyre, V., & Castillo, P. E. (2003). Heterosynaptic LTD of hippocampal GABAergic synapses: a novel role of endocannabinoids in regulating excitability. *Neuron*, *38*(3), 461–472. https://doi.org/10.1016/s0896-6273(03)00235-6

Cichon, J., Gan, WB. Branch-specific dendritic Ca^{2+} spikes cause persistent synaptic plasticity. *Nature* 520, 180–185 (2015). https://doi.org/10.1038/nature14251

Donato, F., Rompani, S. B., & Caroni, P. (2013). Parvalbumin-expressing basket-cell network plasticity induced by experience regulates adult learning. *Nature*, *504*(7479), 272–276. https://doi.org/10.1038/nature12866

Fu, M., Yu, X., Lu, J. *et al.* Repetitive motor learning induces coordinated formation of clustered dendritic spines *in vivo*. *Nature* 483, 92–95 (2012). https://doi.org/10.1038/nature10844

Gambino, F., Pagès, S., Kehayas, V. *et al.* Sensory-evoked LTP driven by dendritic plateau potentials *in vivo*. *Nature* 515, 116–119 (2014). https://doi.org/10.1038/nature13664

Gentet, L., Kremer, Y., Taniguchi, H. *et al.* Unique functional properties of somatostatin-expressing GABAergic neurons in mouse barrel cortex. *Nat Neurosci* 15, 607–612 (2012). https://doi.org/10.1038/nn.3051

Golding, N. L., & Spruston, N. (1998). Dendritic sodium spikes are variable triggers of axonal action potentials in hippocampal CA1 pyramidal neurons. *Neuron*, *21*(5), 1189–1200. https://doi.org/10.1016/s0896-6273(00)80635-2

Golding, N. L., Staff, N. P., & Spruston, N. (2002). Dendritic spikes as a mechanism for cooperative long-term potentiation. *Nature*, *418*(6895), 326–331. https://doi.org/10.1038/nature00854

Guo, J. Z., Graves, A. R., Guo, W. W., Zheng, J., Lee, A., Rodríguez-González, J., Li, N., Macklin, J. J., Phillips, J. W., Mensh, B. D., Branson, K., & Hantman, A. W. (2015). Cortex commands the performance of skilled movement. *eLife*, *4*, e10774. https://doi.org/10.7554/eLife.10774

Harms, K. J., Rioult-Pedotti, M. S., Carter, D. R., & Dunaevsky, A. (2008). Transient spine expansion and learning-induced plasticity in layer 1 primary motor cortex. *The Journal of neuroscience : the official journal of the Society for Neuroscience*, *28*(22), 5686–5690. https://doi.org/10.1523/JNEUROSCI.0584-08.2008

Hayashi-Takagi, A., Yagishita, S., Nakamura, M. *et al.* Labelling and optical erasure of synaptic memory traces in the motor cortex. *Nature* 525, 333–338 (2015). https://doi.org/10.1038/nature15257

Hennequin, G., Agnes, E. J., & Vogels, T. P. (2017). Inhibitory Plasticity: Balance, Control, and Codependence. *Annual review of neuroscience*, *40*, 557–579. https://doi.org/10.1146/annurev-neuro-072116-031005

Hennequin, G., Vogels, T. P., & Gerstner, W. (2014). Optimal control of transient dynamics in balanced networks supports generation of complex movements. *Neuron*, *82*(6), 1394–1406. https://doi.org/10.1016/j.neuron.2014.04.045

Hess, G., & Donoghue, J. P. (1994). Long-term potentiation of horizontal connections provides a mechanism to reorganize cortical motor maps. *Journal of neurophysiology*, *71*(6), 2543–2547. https://doi.org/10.1152/jn.1994.71.6.2543

Holthoff, K., Kovalchuk, Y., Yuste, R., & Konnerth, A. (2004). Single-shock LTD by local dendritic spikes in pyramidal neurons of mouse visual cortex. *The Journal of physiology*, *560*(Pt 1), 27–36. https://doi.org/10.1113/jphysiol.2004.072678

Huber, D., Gutnisky, D., Peron, S. *et al.* Multiple dynamic representations in the motor cortex during sensorimotor learning. *Nature* 484, 473–478 (2012). https://doi.org/10.1038/nature11039

Humeau, Y., & Lüthi, A. (2007). Dendritic calcium spikes induce bi-directional synaptic plasticity in the lateral amygdala. *Neuropharmacology*, *52*(1), 234–243. https://doi.org/10.1016/j.neuropharm.2006.07.010

Inagaki, T., Begum, T., Reza, F., Horibe, S., Inaba, M., Yoshimura, Y., & Komatsu, Y. (2008). Brain-derived neurotrophic factor-mediated retrograde signaling required for the induction of

long-term potentiation at inhibitory synapses of visual cortical pyramidal neurons. *Neuroscience research*, *61*(2), 192–200. https://doi.org/10.1016/j.neures.2008.02.006

Jia, H., Rochefort, N., Chen, X. *et al.* Dendritic organization of sensory input to cortical neurons *in vivo*. *Nature* 464, 1307–1312 (2010). https://doi.org/10.1038/nature08947

Kano, M., Kano, M., Fukunaga, K., & Konnerth, A. (1996). Ca (2+)-induced rebound potentiation of gamma-aminobutyric acid-mediated currents requires activation of Ca2+/calmodulin-dependent kinase II. *Proceedings of the National Academy of Sciences of the United States of America*, *93*(23), 13351–13356. https://doi.org/10.1073/pnas.93.23.13351

Kampa, B. M., Letzkus, J. J., & Stuart, G. J. (2006). Requirement of dendritic calcium spikes for induction of spike-timing-dependent synaptic plasticity. *The Journal of physiology*, *574*(Pt 1), 283–290. https://doi.org/10.1113/jphysiol.2006.111062

Kawai, R., Markman, T., Poddar, R., Ko, R., Fantana, A. L., Dhawale, A. K., Kampff, A. R., & Ölveczky, B. P. (2015). Motor cortex is required for learning but not for executing a motor skill. *Neuron*, *86*(3), 800–812. https://doi.org/10.1016/j.neuron.2015.03.024

Kepecs, A., Fishell, G. Interneuron cell types are fit to function. *Nature* 505, 318–326 (2014). https://doi.org/10.1038/nature12983

Kole, M. H., Letzkus, J. J., & Stuart, G. J. (2007). Axon initial segment Kv1 channels control axonal action potential waveform and synaptic efficacy. *Neuron*, *55*(4), 633–647. https://doi.org/10.1016/j.neuron.2007.07.031

Komiyama, T., Sato, T., O'Connor, D. *et al.* Learning-related fine-scale specificity imaged in motor cortex circuits of behaving mice. *Nature* 464, 1182–1186 (2010). https://doi.org/10.1038/nature08897

Larkum, M., Zhu, J. & Sakmann, B. A new cellular mechanism for coupling inputs arriving at different cortical layers. *Nature* 398, 338–341 (1999). https://doi.org/10.1038/18686

Laubach, M., Wessberg, J. & Nicolelis, M. Cortical ensemble activity increasingly predicts behaviour outcomes during learning of a motor task. *Nature* 405, 567–571 (2000). https://doi.org/10.1038/35014604

Lavzin, M., Rapoport, S., Polsky, A. *et al.* Nonlinear dendritic processing determines angular tuning of barrel cortex neurons *in vivo*. *Nature* 490, 397–401 (2012). https://doi.org/10.1038/nature11451

Lien, CC., Mu, Y., Vargas-Caballero, M. *et al.* Visual stimuli–induced LTD of GABAergic synapses mediated by presynaptic NMDA receptors. *Nat Neurosci* 9, 372–380 (2006). https://doi.org/10.1038/nn1649

Lin, Y., Bloodgood, B. L., Hauser, J. L., Lapan, A. D., Koon, A. C., Kim, T. K., Hu, L. S., Malik, A. N., & Greenberg, M. E. (2008). Activity-dependent regulation of inhibitory synapse development by Npas4. *Nature*, *455*(7217), 1198–1204. https://doi.org/10.1038/nature07319

Longordo, F., To, MS., Ikeda, K. *et al.* Sublinear integration underlies binocular processing in primary visual cortex. *Nat Neurosci* 16, 714–723 (2013). https://doi.org/10.1038/nn.3394

Losonczy, A., & Magee, J. C. (2006). Integrative properties of radial oblique dendrites in hippocampal CA1 pyramidal neurons. *Neuron*, *50*(2), 291–307. https://doi.org/10.1016/j.neuron.2006.03.016

Masamizu, Y., Tanaka, Y. R., Tanaka, Y. H., Hira, R., Ohkubo, F., Kitamura, K., Isomura, Y., Okada, T., & Matsuzaki, M. (2014). Two distinct layer-specific dynamics of cortical ensembles during learning of a motor task. *Nature neuroscience*, *17*(7), 987–994. https://doi.org/10.1038/nn.3739

Murayama, M., & Larkum, M. E. (2009). Enhanced dendritic activity in awake rats. *Proceedings of the National Academy of Sciences of the United States of America*, *106*(48), 20482–20486. https://doi.org/10.1073/pnas.0910379106

Murphy, B. K., & Miller, K. D. (2009). Balanced amplification: a new mechanism of selective amplification of neural activity patterns. *Neuron*, *61*(4), 635–648. https://doi.org/10.1016/j.neuron.2009.02.005

Nugent, F. S., Penick, E. C., & Kauer, J. A. (2007). Opioids block long-term potentiation of inhibitory synapses. *Nature*, *446*(7139), 1086–1090. https://doi.org/10.1038/nature05726

Otchy, T. M., Wolff, S. B., Rhee, J. Y., Pehlevan, C., Kawai, R., Kempf, A., Gobes, S. M., & Ölveczky, B. P. (2015). Acute off-target effects of neural circuit manipulations. *Nature*, *528*(7582), 358–363. https://doi.org/10.1038/nature16442

Ouardouz, M., & Sastry, B. R. (2000). Mechanisms underlying LTP of inhibitory synaptic transmission in the deep cerebellar nuclei. *Journal of neurophysiology*, *84*(3), 1414–1421. https://doi.org/10.1152/jn.2000.84.3.1414

Palmer, L., Shai, A., Reeve, J. *et al.* NMDA spikes enhance action potential generation during sensory input. *Nat Neurosci* 17, 383–390 (2014). https://doi.org/10.1038/nn.3646

Peters, A. J., Chen, S. X., & Komiyama, T. (2014). Emergence of reproducible spatiotemporal activity during motor learning. *Nature*, *510*(7504), 263–267. https://doi.org/10.1038/nature13235

Peters, A., Lee, J., Hedrick, N. *et al.* Reorganization of corticospinal output during motor learning. *Nat Neurosci* 20, 1133–1141 (2017). https://doi.org/10.1038/nn.4596

Polsky, A., Mel, B. & Schiller, J. Computational subunits in thin dendrites of pyramidal cells.*Nat Neurosci* 7, 621–627 (2004). https://doi.org/10.1038/nn1253

Remy, S., & Spruston, N. (2007). Dendritic spikes induce single-burst long-term potentiation. *Proceedings of the National Academy of Sciences of the United States of America*, *104*(43), 17192–17197. https://doi.org/10.1073/pnas.0707919104

Schiller, J., Major, G., Koester, H. *et al.* NMDA spikes in basal dendrites of cortical pyramidal neurons. *Nature* 404, 285–289 (2000). https://doi.org/10.1038/35005094

Sheffield, M., Dombeck, D. Calcium transient prevalence across the dendritic arbour predicts place field properties. *Nature* 517, 200–204 (2015). https://doi.org/10.1038/nature13871

Smith, S. L., Smith, I. T., Branco, T., & Häusser, M. (2013). Dendritic spikes enhance stimulus selectivity in cortical neurons in vivo. *Nature*, *503*(7474), 115–120. https://doi.org/10.1038/nature12600

Stuart, G., Spruston, N., Sakmann, B., & Häusser, M. (1997). Action potential initiation and backpropagation in neurons of the mammalian CNS. *Trends in neurosciences*, *20*(3), 125–131. https://doi.org/10.1016/s0166-2236(96)10075-8

Takahashi, N., Kitamura, K., Matsuo, N., Mayford, M., Kano, M., Matsuki, N., & Ikegaya, Y. (2012). Locally synchronized synaptic inputs. *Science (New York, N.Y.)*, *335*(6066), 353–356. https://doi.org/10.1126/science.1210362

Tremblay, R., Lee, S., & Rudy, B. (2016). GABAergic Interneurons in the Neocortex: From Cellular Properties to Circuits. *Neuron*, *91*(2), 260–292. https://doi.org/10.1016/j.neuron.2016.06.033

Vogels, T. P., Sprekeler, H., Zenke, F., Clopath, C., & Gerstner, W. (2011). Inhibitory plasticity balances excitation and inhibition in sensory pathways and memory networks. *Science (New York, N.Y.)*, *334*(6062), 1569–1573. https://doi.org/10.1126/science.1211095

Woodin, M. A., Ganguly, K., & Poo, M. M. (2003). Coincident pre- and postsynaptic activity modifies GABAergic synapses by postsynaptic changes in Cl- transporter activity. *Neuron*, *39*(5), 807–820. https://doi.org/10.1016/s0896-6273(03)00507-5

Xu, N. L., Harnett, M. T., Williams, S. R., Huber, D., O'Connor, D. H., Svoboda, K., & Magee, J. C. (2012). Nonlinear dendritic integration of sensory and motor input during an active sensing task. *Nature*, *492*(7428), 247–251. https://doi.org/10.1038/nature11601

Xu, T., Yu, X., Perlik, A. *et al.* Rapid formation and selective stabilization of synapses for enduring motor memories. *Nature* 462, 915–919 (2009). https://doi.org/10.1038/nature08389

Yang, G., Pan, F., & Gan, W. B. (2009). Stably maintained dendritic spines are associated with lifelong memories. *Nature*, *462*(7275), 920–924. https://doi.org/10.1038/nature08577

Yang, J., Serrano, P., Yin, X., Sun, X., Lin, Y., & Chen, S. X. (2022). Functionally distinct NPAS4-expressing somatostatin interneuron ensembles critical for motor skill learning. *Neuron*, *110*(20), 3339–3355.e8. https://doi.org/10.1016/j.neuron.2022.08.018